

UNSW

AUSTRALIA

SCHOOL OF ELECTRICAL ENGINEERING AND TELECOMMUNICATIONS

Power-Efficient SISO-NOMA System Assisted by Passive STAR-IRS: Optimization and Performance Analysis

by

Lanke CHEN

Thesis submitted as a requirement for the degree

Master of Engineering (Telecommunications)

Submitted: Oct. 20, 2026

Supervisor: Derrick Wing Kwan Ng

Abstract

This thesis examines a power-efficient downlink transmission strategy for a simultaneously transmitting and reflecting intelligent reflecting surface (STAR-IRS) supported single-input single-output non-orthogonal multiple access (SISO-NOMA) system and assesses its performance via optimization and simulation. Utilizing a passive STAR-IRS, a singular metasurface may concurrently accommodate users positioned on either side of the surface, thus mitigating line-of-sight obstructions and enhancing cell-edge coverage. NOMA is implemented to enable numerous users to utilize the same time-frequency resource, employing a predetermined successive interference cancellation (SIC) decoding order based on effective channel gains. Utilizing a comprehensive signal model, signal-to-interference-plus-noise ratio (SINR) expressions, and a pragmatic power-consumption model, we establish a total transmit-power minimization problem constrained by quality of service (QoS), power budget, and successive interference cancellation (SIC) decodability requirements, along with discrete phase-shift limitations at the STAR-IRS.

An alternating optimization framework is established to address this non-convex problem. A closed-form solution for base-station power allocation is derived for a specified STAR-IRS phase vector by utilizing the structure of the SINR restrictions. For fixed power, a continuous STAR-IRS phase design is obtained via a gradient-aligned refinement of the cascaded channels, followed by 2-bit quantization and local combinatorial refinement to satisfy discrete hardware constraints. Numerical results indicate that the proposed discrete STAR-IRS-assisted approach significantly decreases the necessary base station transmit power in comparison to systems lacking IRS, those utilizing conventional IRS, and those employing random STAR-IRS phases, while attaining performance around the continuous-phase upper limit. Furthermore, the proposed algorithm exhibits fast convergence and low computational complexity, making it suitable for future low-power 6G wireless networks.

Abbreviations

5G Fifth generation

6G Sixth generation

AO Alternating Optimization

AWGN Additive White Gaussian Noise

BS Base Station

CSI Channel State Information

IRS Intelligent Reflecting Surface

LoS Line-of-Sight

MC Monte-Carlo

SISO Single-Input Single-Output

NOMA Non-Orthogonal Multiple Access

QoS Quality of Service

SIC Successive Interference Cancellation

SINR Signal-to-Interference-plus-Noise Ratio

STAR-IRS Simultaneously Transmitting and Reflecting Intelligent Reflecting Surface

IoT Internet of Things

OMA Orthogonal Multiple Access

TDMA Time Division Multiple Access

FDMA Frequency Division Multiple Access

OFDMA Orthogonal Frequency Division Multiple Access

NLoS Non-Line-of-Sight

List of Symbols

K Total number of users in the system

K_r, K_t Number of users in reflection and transmission zones, respectively

$\mathcal{K}_R, \mathcal{K}_T$ Index sets of reflection and transmission users, respectively

N Number of passive STAR-IRS elements

t AO iteration index

p_k Power allocated to user k

$\mathbf{p} = [p_1, \ldots, p_K]$ Power allocation vector at the BS

$p_{\max}$ Total transmit power constraint at the BS

P_{BS} Total BS transmit power

P_{IRS} Total control power consumed by STAR-IRS

P_{unit} Control power per IRS element

P_{tot} Total system power consumption (BS transmit power plus STAR-IRS control power)

σ^2 Noise power (variance of AWGN)

n_k AWGN at user k, with distribution $n_k \sim \mathcal{CN}(0, \sigma^2)$

s_k Unit-power modulated signal intended for user k

x Superposed NOMA signal transmitted by the BS

$h_{d,k}$ Direct channel gain from BS to user k

$\boldsymbol{g}$ Channel vector from BS to STAR-IRS, $\boldsymbol{g} \in \mathbb{C}^{N \times 1}$

$\boldsymbol{h}_k^{(r)}$ Channel vector from STAR-IRS (reflection side) to user k

$\boldsymbol{h}_k^{(t)}$ Channel vector from STAR-IRS (transmission side) to user k

$\boldsymbol{\Theta}_r$ Reflection phase shift matrix of STAR-IRS,$\boldsymbol{\Theta}_r \in \mathbb{C}^{N\times N}$

$\boldsymbol{\Theta}_t$ Transmission phase shift matrix of STAR-IRS,$\boldsymbol{\Theta}_t \in \mathbb{C}^{N\times N}$

δ_n Power-splitting coefficient of IRS element n, $\delta_n \in [0,1]$

θ_n^r, θ_n^t Discrete phase shifts for reflection/transmission at element n

$h_k^{(r)}, h_k^{(t)}$ Cascaded STAR-IRS-assisted channels for reflection-side and transmission-side user k, respectively

h_k^{eff} Total effective channel between the BS and user k, including both direct and STAR-IRS-assisted links

y_k Received signal at user k

γ_k^{min} Minimum SINR threshold required for user k' s QoS

SINR_k Signal-to-Interference-plus-Noise Ratio of user k' s own signal

$\text{SINR}_{k\to j}$ SINR for user k decoding user j' s signal (in SIC)

$\text{PL}(d)$ Large-scale path loss function depending on distance d

PL_0 Reference path loss at a distance of 1 m

α Path loss exponent

$f(\cdot)$ Objective function

d_{BI} BS-to-IRS distance

d_{IU} IRS-to-User distance

ϕ STAR-IRS phase-shift vector

ϵ AO convergence tolerance

Contents

Abstract I

Abbreviations II

List of symbols IV

Contents VI

1 Introduction 1

2 Literature Review 3

2.1 IRS and STAR-IRS Technology 3

2.2 NOMA 5

2.3 Integration of IRS/STAR-IRS with NOMA 7

2.4 Low-Power Optimization Approaches in 6G Networks 8

3 System Model and Problem Formulation 11

3.1 System Model Description 11

3.2 Channel and Link Modeling 12

3.2.1 Direct Link: Base Station to User Channel $h_{d,k}$ 13

3.2.2 STAR-IRS Links: BS-IRS and IRS-User Channels 13

3.2.3 STAR-IRS Phase Shift Matrices 14

3.2.4 Composite IRS-assisted Channels 14

3.2.5 Total Effective Channel 15

3.3 Joint Signal Modeling 15
3.4 Detailed SINR Derivation 15
3.4.1 SINR for Decoding a Weaker User's Signal 16
3.4.2 SINR for Decoding the Intended Signal 17
3.5 Power Consumption Model 17
3.6 Optimization Constraints 18
3.7 Mathematical Problem Formulation 18

4 Proposed Solution **20**
4.1 Overview of the Optimization Framework 20
4.2 Power Allocation Subproblem 20
4.3 STAR-IRS Phase Design Subproblem 22
4.3.1 Continuous Relaxation and Quantization 22
4.3.2 Discrete Coordinate Descent 23
4.4 Alternating Optimization Algorithm 24
4.5 Convergence and Complexity Analysis 24

5 Simulation and Results **26**
5.1 Simulation Setup 26
5.2 Simulation Results 27
5.3 Summary of Findings 34

6 Conclusion and Future Work **36**
6.1 Conclusion 36
6.2 Future Work 37

Bibliography **38**

Chapter 1

Introduction

Anticipated sixth-generation (6G) wireless networks are projected to significantly enhance energy efficiency, network capacity, coverage, and Quality of Service (QoS) for a vast array of devices and applications [1-5]. Simultaneously, evolving contexts like smart cities, the industrial Internet of Things (IoT), and edge computing necessitate rigorous standards for reliability and low-power functionality. Conventional infrastructure dependent on active relays, energy-intensive radio-frequency chains, and intricate signal processing may result in significant energy usage, particularly in densely populated deployments. These issues necessitate the advancement of sophisticated wireless architectures to improve the quality of wireless connections without augmenting transmission power or hardware expenses [1, 5-7].

Recently, energy-efficient wireless networks have begun to introduce intelligent reflecting surface (IRS) technology. An IRS uses many passive, reconfigurable elements to change its electromagnetic response, and it can modify the wireless propagation environment with little energy [8-12]. Taking this idea, the simultaneously transmitting and reflecting IRS (STAR-IRS) extends the coverage to both sides of the surface by individually controlling the reflective and transmitting parts respectively [6, 13-15]. Double-sided coverage enhances the flexibility and availability of deployment in the blockage obstacle environment [15, 16].

Non-orthogonal multiple access (NOMA) has become another way to increase bandwidth and meet the demand for massive connectivity [2-4]. Multiple users compete for the same time-frequency resource block, where their signals are multiplexed in the power domain and successively processed by successive interference cancellation (SIC) at the receiver. In this way, NOMA can further increase throughput and become more robust under heterogeneous channel

conditions. The integration of NOMA with IRS or STAR-IRS accentuates the interdependence of power allocation, user decoding sequence, and passive beamforming design, while discrete hardware limitations further complicate the resolution of these issues [1, 17-29].

Motivated by these problems, this thesis takes the downlink single input single output (SISO) NOMA system assisted by passive STAR-IRS as the research object to achieve full-space user coverage and low power consumption [13, 25, 26, 29]. A predetermined global SIC decoding sequence is utilized for simplicity and signaling efficiency, but practical discrete phase shifts are mandated at the STAR-IRS to guarantee implement ability. The primary aim is to collaboratively optimize the transmit power allocation of the base station and the phase-shift configuration of the STAR-IRS, while adhering to users' QoS requirements, total power limitations, and SIC decidability.

This thesis's principal contributions can be succinctly stated as follows. Initially, a comprehensive power-efficient optimization framework [21-23, 30, 31] is developed for STAR-IRS-assisted SISO-NOMA downlink communications with a practical 2-bit phase-shift constraint [32-36]. The proposed method incorporates a realistic STAR-IRS hardware power model and a fixed global SIC decoding order that avoids frequent reconfiguration, ensuring a balance between performance and practical signaling overhead. Second, a closed-form power allocation solution is derived by exploiting the recursive structure of the SINR constraints, providing a low-complexity and near-optimal update for the transmit power in each iteration. Third, an efficient alternating optimization strategy [19, 22-24, 26, 37, 38] is proposed for discrete-phase STAR-IRS design, combining gradient-aligned continuous phase refinement with quantization and local combinatorial improvement over a small subset of dominant elements. Finally, extensive simulations are performed under varying IRS sizes, QoS constraints, geometry conditions and user distributions, demonstrating that the proposed discrete STAR-IRS achieves substantial and consistent power savings with fast convergence and significantly reduced complexity compared with continuous-phase designs and existing benchmarks.

Overall, this thesis establishes a practical and effective STAR-IRS-assisted NOMA system design approach that enhances energy efficiency and maintains near-optimal beamforming performance under realistic hardware limitations. The proposed framework and findings provide valuable guidance for the deployment of cost-effective intelligent surfaces in future 6G networks.

Chapter 2

Literature Review

2.1 IRS and STAR-IRS Technology

Reconfigurable intelligent surfaces (RISs), also termed intelligent reflecting surfaces (IRSs), aim to shape the radio propagation environment through electronically controllable electromagnetic responses. Unlike a conventional active relay, an ideally passive IRS neither decodes and forwards the user message nor employs an RF power amplifier. Its elements instead re-radiate incident fields with adjustable phase and, depending on the hardware, adjustable amplitude. Foundational analyses explain why the resulting cascaded channel can improve link quality and coverage, while emphasizing that propagation losses across the base-station-to-surface and surface-to-user hops cannot be ignored [5, 8, 9]. These distinctions are important for energy-efficiency comparisons: passive surface operation does not imply zero control, bias, signaling, or channel-acquisition power [10-12, 59].

A conventional reflecting-only IRS predominantly serves users on the illuminated side of the surface. Simultaneously transmitting and reflecting RISs (STAR-RISs, also called STAR-IRSs) extend this mechanism by supporting reflected and transmitted electromagnetic responses [6, 13-16]. Energy-splitting, mode-switching, and time-switching protocols offer different trade-offs between concurrent service, hardware complexity, and scheduling flexibility. The distinction is not only geometric: the reflection-side and transmission-side channels share an incident wave and, in practical realizations, may be constrained by amplitude conservation, phase coupling, insertion loss, and limited-resolution tuning. Consequently, optimizing two independent phase matrices without acknowledging the physical coupling can describe an idealized rather than a generally implementable device [13, 16, 43, 44, 106].

Subsequent research in 2026 broadens STAR-RIS beyond the narrowband passive downlink model. Wang et al. address active STAR-RIS-assisted wireless-powered communication networks, where amplified surface noise and power supply constraints affect the energy budget [83]. Zhou et al. study robust beamforming in hybrid-field STAR-RIS integrated sensing-and-communication systems [84]. Ranjan et al. examine robust STAR-RIS-assisted multiuser MIMO sensing-and-communication designs [85], and Zhou et al. investigate wideband cell-free ISAC with joint resource allocation and beamforming [86]. These advances supply strong related context for full-space service, but their multi-antenna, sensing, active-device, or wideband assumptions prevent direct one-to-one comparison with the fixed-phase, passive SISO-NOMA system analyzed here.

The STAR-RIS architecture is particularly relevant to dense indoor deployments and obstructed outdoor coverage, because one strategically placed surface can establish additional propagation

paths toward receivers on both sides. Nevertheless, the gain depends on the placement, aperture, blocked-link statistics, user geometry, and channel coherence. Greater element count does not always produce a proportionate reduction in total system power: additional elements increase control overhead and create more channel parameters that must be learned and updated [8, 11, 39, 89]. Similarly, the choice between passive and active surfaces is an energy-budget decision rather than a universal hierarchy. An active STAR-RIS can compensate for some cascaded-link loss through amplification, but it also introduces amplifier noise and consumption; active STAR-RIS-aided wireless-powered networks illustrate these different physical and optimization regimes [10-12, 83].

A growing body of work considers multidimensional IRS and STAR-RIS operation rather than only an ideal narrowband reflecting link. In 'Dual-Sided Active Intelligent Reflecting Surface-Enhanced Multi-Cell Communications,' Liu et al. investigate dual-sided coverage with active elements [82]. Deshpande et al. analyze energy-efficient STAR-RIS-aided multiuser MIMO for ultra-reliable low-latency communication (URLLC), exposing a balance between surface control, transmit resources, and stringent reliability demands [79]. Research on coupled transmissive/reflective elements under spatially correlated angular uncertainty similarly emphasizes physical constraints that are often absent from elementary phase-only models [106]. These studies motivate the two-region topology of the present thesis, but they also make clear that its passive SISO energy-splitting abstraction should not be conflated with active, MIMO, or electromagnetically coupled hardware.

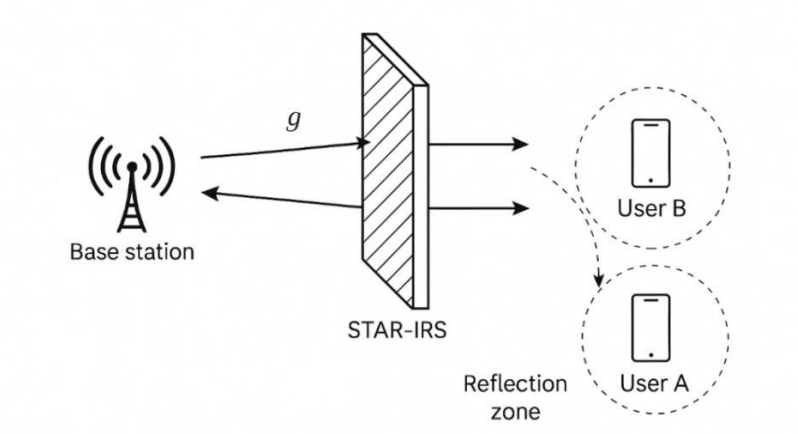

Figure 2.1: STAR-IRS simultaneously serving users on both sides.

Channel acquisition remains a major implementation bottleneck. Because a passive surface typically lacks conventional baseband receive chains, estimating the cascaded BS-IRS-user links generally requires structured pilots, element grouping, compressed-sensing methods, or auxiliary sensing elements [32, 46-48]. Chu et al. develop a partially decoupled atomic-norm approach for RIS-aided MIMO channel estimation [102]; Cao et al. investigate semi-passive elements for massive access [111]. Channel-aging-aware precoding and cell-free RIS results further demonstrate that a phase profile optimized for outdated CSI may underperform under user mobility [103, 105]. Such work supports the thesis's decision to study a tractable ideal-CSI

baseline, but it identifies an important gap between the model and a deployable low-complexity controller.

Hardware phase quantization adds a separate non-convex constraint. Two-bit phase control restricts each programmed angle to one of four states, so an unconstrained continuous-phase optimum generally cannot be implemented directly [32-36]. Wu et al. specifically address globally optimal resource allocation for discrete-phase IRS multiuser networks with both perfect and imperfect CSI [100]. Their globally optimal formulation establishes a useful methodological reference: a quantized heuristic should be evaluated against a rigorous discrete-phase benchmark where computationally feasible, not only against random phases or a relaxed continuous solution. Codebook-based RIS designs provide another implementation-oriented direction, trading online search for pre-computed, possibly geometry-dependent phase configurations [101]. The present thesis adopts a low-complexity quantization and refinement approach; it does not claim global optimality of the resulting discrete phases.

2.2 Power-Domain NOMA and Resource Allocation

Power-domain non-orthogonal multiple access (NOMA) superposes multiple users' data streams within a common time-frequency resource. In a conventional downlink, users are distinguished through transmit power assignment and successive interference cancellation (SIC), whereby a receiver may first decode selected other users' messages and remove them before recovering its own message [2, 3]. The benefits are conditional on the propagation asymmetry, decoding order, receiver complexity, CSI accuracy, and target metric. NOMA should therefore be compared with an appropriately optimized orthogonal multiple access (OMA) baseline rather than being treated as uniformly more energy-efficient [64, 65].

Ng and coauthors have developed multiple lines of work on NOMA's performance and resource-management fundamentals. Wei et al. compare the performance gain of NOMA over OMA in uplink communications [65]. For multicarrier NOMA with imperfect CSI, Wei et al. formulate optimal resource allocation with explicit power-efficiency considerations [66]. Sun et al. jointly optimize downlink beamforming and user power allocation in multiuser MIMO-NOMA [67], while Wang et al. propose minimum-error-probability NOMA design principles [68]. Taken together, these studies show why a rate expression or a fixed power ordering alone is insufficient to establish energy efficiency: interference, decoding feasibility, channel uncertainty, and the actual objective must be handled jointly.

The practical SIC receiver imposes constraints that are easy to overlook in a theoretical power-allocation derivation. Under a fixed global order, the transmitter must allocate sufficient power not only for each receiver's own SINR but also for each stronger receiver to decode the messages it cancels. Noise enhancement, channel-estimation errors, and residual SIC interference may alter this feasibility region. Joint pilot and payload power control for MIMO-NOMA with MRC-SIC receivers explores the training-resource dimension [69]; NOMA-based cell-free massive MIMO for Internet-of-Things (IoT) demonstrates how distributed architectures change the interference

and serving-set assumptions [70]. Faster-than-Nyquist asynchronous NOMA offers yet another example in which timing assumptions materially influence achievable rates [71].

Spatial techniques can strengthen or diminish the attractiveness of power-domain NOMA. Hybrid millimeter-wave NOMA with beamwidth control [72] and multi-beam NOMA [73] exploit directional separation rather than relying exclusively on channel-gain disparity. Their results are not directly transferrable to a single-antenna BS, which has no independent active-beamforming vectors. However, these studies highlight why extending the present SISO setting to MIMO would fundamentally alter the joint optimization space. More recently, a broad survey synthesizes NOMA's progress and limitations for next-generation multiple access [64]; a movable-antenna-enhanced downlink NOMA study explores additional spatial adaptation [98].

For the thesis's SISO downlink, the specific value of NOMA is to support multiple users with one radiated composite signal and to permit a low-dimensional power-update subproblem. It is not correct to assume that NOMA automatically reduces instantaneous BS transmit power. Whether NOMA is preferable depends on the target QoS levels and the OMA benchmark's resource allocation, scheduling fraction, and receiver complexity. A credible comparison must hold bandwidth, user-rate demand, channel realization, and power-consumption accounting consistent [21-24, 74].

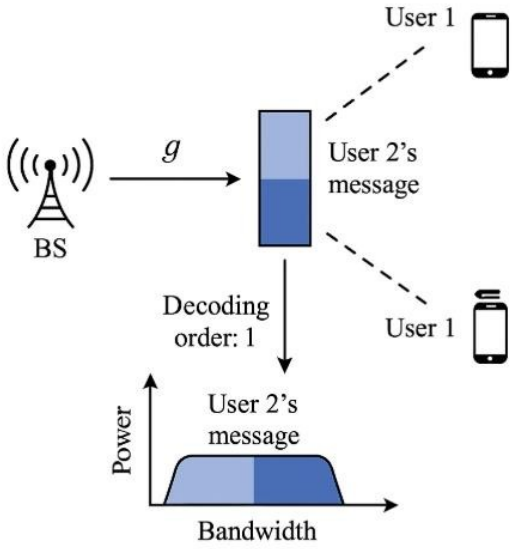

Figure 2.2: Downlink NOMA power-domain multiplexing and SIC.

2.3 Integration of IRS/STAR-IRS With NOMA

The joint use of IRSs and NOMA introduces a coupled passive-beamforming and power-allocation problem: a surface modifies each user's effective channel, while the resulting relative channel strengths and SINR margins influence which NOMA decoding order is feasible [1, 17-24]. A stronger reflected path can lower the power needed to meet a weak user's QoS constraint, but it can also change channel ordering or increase the interference suffered by other users.

Consequently, it is not generally valid to optimize the IRS toward one user independently of the complete SIC chain.

Early IRS-NOMA investigations established basic outage, rate, and power-allocation behavior and showed that continuous and discrete phase designs can behave differently [17-24, 54]. In power-minimization formulations, the phase variables affect not only the desired signal powers but also the noise-normalized interference terms at all relevant SIC receivers. The feasibility of SIC must therefore be evaluated after each substantial phase update. If a decoding order is determined from a reference channel realization and subsequently held fixed, its assumed channel-gain ordering may cease to hold after surface reconfiguration. The algorithm must either maintain the ordering with explicit constraints or verify the complete SIC inequalities for every candidate configuration [22, 24, 25].

STAR-RIS-aided NOMA generalizes this joint design to users in reflection and transmission regions. Mu et al. introduce the basic STAR-RIS signal modeling framework, while subsequent work studies throughput, outage, secrecy, and power control under various surface protocols [6, 13-16, 25-29, 37, 38, 55-58]. The surface's energy-splitting ratios determine the available amplitudes of the two links, and the reflection/transmission phase coefficients create a trade-off across the two user groups. Assuming independent reflection and transmission phases is a useful relaxation only when the selected physical hardware supports sufficient independent control [13, 29, 106].

Feng et al. investigate rate enhancement for STAR-RIS-assisted uplink NOMA [77], which is directly connected to the present technology combination but differs in traffic direction, interference structure, and SIC order. Singh et al. study adaptive neural-network optimization for fully connected STAR-RIS-aided NOMA [78], illustrating a broader, more hardware-general coupling model and an alternative to deterministic local search. Research on covert and secrecy performance of RIS-NOMA links addresses additional security objectives rather than the minimum BS power considered here [95]. A study of RIS-aided NOMA with integrated sensing in a satellite network provides a more recent application-specific extension [96].

Work on related combinations helps isolate the contribution of the present study. Cai et al. jointly optimize an IRS-assisted UAV-NOMA link and the UAV's three-dimensional trajectory for power efficiency [76], introducing movement and geometry optimization absent from this thesis. Chen et al. compare TDMA and NOMA for IRS-assisted wireless-powered mobile-edge computation [75], showing that the preferable access method depends on energy transfer and computation constraints. Zhang et al. investigate SWIPT-enabled cell-free MIMO-NOMA with machine learning [99], where distributed active transmitters and wireless powering create additional degrees of freedom. Pattern-domain NOMA for OTFS modulation changes the multiplexing domain and receiver assumptions [97]. These are meaningful extensions, not directly comparable numerical baselines for a fixed-location passive STAR-RIS SISO downlink.

A distinct stream of STAR-RIS work optimizes security or joint sensing and communications rather than minimum downlink transmit power. Zhang et al. compare decoupled optimization and learning-based approaches for STAR-RIS-aided ISAC [80]; Wang et al. combine a STAR-RIS with secure dual-functional radar-communications waveform design [81]. Zheng et al. analyze reconfigurable-surface-aided secure integrated radar and communication systems [94]. In each case, adding sensing discrimination, secrecy, or waveform requirements changes the feasible set and performance metric. These contributions strengthen the architectural literature, but their objectives should be differentiated from the NOMA QoS-and-SIC constraints imposed in the present thesis.

The precise research gap considered in this thesis is narrower than the full STAR-RIS/NOMA literature. The BS has a single antenna; users are served in one downlink NOMA resource block; a fixed global SIC order reduces signaling complexity; and the passive STAR-IRS is programmed using practical two-bit phases. The design minimizes BS transmit power plus a stated surface-control term subject to user-QoS, SIC, and BS power-budget constraints. The main difficulty is the feedback between the discrete surface responses and the required NOMA powers, particularly when two-sided users compete for the same incident energy. The thesis therefore examines alternating closed-form power updates with discrete phase refinement rather than solving the more general MIMO, active-surface, or joint-decoding-order problems.

2.4 Low-Power Optimization Approaches in 6G Networks

Energy-efficient wireless design requires careful differentiation among transmit-power minimization, total consumed-power minimization, and energy-efficiency maximization. The first minimizes radiated power under fixed QoS constraints; the second also accounts for circuitry, processing, control, and possibly amplifier inefficiency; the third typically maximizes delivered information per joule. All three can lead to different surface sizes, power allocations, and feasible deployment choices [8, 10-12, 21-24]. In the present thesis, the stated control-power model is N times a per-element constant. For a fixed N, that term does not affect the phase optimizer, although it does matter when evaluating the net benefit of increasing N. This distinction is essential when interpreting the numerical curves.

Wei et al. address optimal power-efficient multicarrier NOMA under imperfect CSI [66], and Wu et al. examine when a wireless-powered IoT system should prefer NOMA over TDMA [74]. Sun et al. optimize beamforming and power jointly in MIMO-NOMA [67], while the energy-efficient design of STAR-RIS-aided URLLC systems extends the objective to tight reliability constraints [79]. These papers collectively motivate QoS-constrained power minimization, but their optimization variables and service metrics differ.

Several modern RIS studies approach the same energy question from complementary perspectives. Wu et al.'s globally optimal solution for discrete-phase IRS [100] provides a discrete

nonconvex-optimization reference. Wang et al. analyze IRS energy efficiency under statistical QoS constraints, showing why average-rate targets and delay-related statistical guarantees should not be conflated [89]. Zhao et al. investigate RIS-aided energy-efficient mobile-edge computing in OFDM systems [92], while Lu et al. survey energy-efficient RIS-aided cell-free massive MIMO architectures [108]. Another recent study jointly performs RIS-assisted distributed precoding and access-point selection with multi-agent reinforcement learning, a high-dimensional network-wide setting [87]. The present thesis instead prioritizes a simple implementation using a single BS transmit chain.

Alternating optimization (AO) is widely employed when powers and passive phases are individually more tractable than the coupled problem [9, 19, 21-24]. Typical ingredients include exact or convex power updates; successive convex approximation, semidefinite relaxation, or penalty methods for surface coefficients; projection onto discrete hardware states; and coordinate descent over individual phase variables. The quality of the AO solution depends on initialization and the block-update policy. A continuous relaxation offers a reference or warm start but is not itself a feasible two-bit design. Nearest-neighbor quantization need not preserve monotonic descent or SIC feasibility; post-quantization objective checks and explicit feasibility tests are therefore necessary [32, 35, 100, 101].

Data-driven alternatives can reduce online search or predict useful configurations from contextual information, but they require training, additional inputs, and robustness evaluation outside the measured channel distribution. Examples include deep-reinforcement-learning optimization of RIS-aided cell-free massive MIMO [88], sensing-based predictive beamforming for vehicular IRS-assisted links [93], and active-IRS resource allocation using a learning-based policy [107]. Such approaches complement but do not negate the value of a transparent physics-based alternating scheme. For a modest passive surface under slowly varying CSI, a verified low-dimensional coordinate update can be preferable to a large inference pipeline.

For distributed architectures, joint RIS-aided precoding and beamforming in cell-free massive MIMO [109] requires cooperation among many active transceivers; its computational architecture does not transfer directly to one SISO base station. Machine-learning-based energy-efficiency optimization of RIS-assisted simultaneous wireless information-and-power transfer [110] likewise includes energy-harvesting constraints that are absent here. These examples show why a literature comparison should align the power objective and service constraints, not merely the presence of a RIS.

Robustness is another central distinction. Beamforming for RIS-assisted cell-free systems with CSI uncertainties and constrained backhaul [104], channel-aging-aware RIS precoding [103], and outdated-CSI wireless-powered RIS communication [112] demonstrate different mechanisms through which nominal-CSI designs can lose performance. Semi-passive surface hardware [111] may simplify channel acquisition but requires nonzero sensing hardware power. Recent STAR-RIS-enabled ISAC results also optimize sensing metrics alongside communication [80, 81, 84, 85,

86], whereas the current SISO-NOMA formulation does not include a sensing requirement. These works clarify meaningful next steps without obscuring the scope of the existing project.

Finally, newer architectures highlight the broader trade-off between propagation reconfiguration and RF-chain resources. Fluid-antenna/RIS multiuser systems combine movable spatial sampling with surface design [90]; asynchronous beamforming for beyond-diagonal RIS networks introduces inter-element coupling [91]. Such configurations can be more capable but require substantially different electromagnetic and optimization models. The thesis focuses instead on a defensible low-complexity baseline that is directly comparable with no-IRS, reflecting-only IRS, random STAR-RIS, and continuous-phase STAR-RIS references, provided the compared designs use consistent user locations, CSI, power accounting, and feasible SIC constraints.

In summary, three gaps motivate the analysis in Chapters 3-5. First, the joint power and phase design must respect the two-sided energy allocation and the fixed NOMA SIC order. Second, finite-resolution hardware creates a combinatorial problem for which a low-complexity but feasibility-preserving method is desirable. Third, a fair power-saving claim must include the surface-control overhead and must not treat a continuous-phase benchmark as an achievable hardware configuration. Within these clearly stated assumptions, the proposed alternating strategy is intended as an engineering approximation, not as a globally optimal or universally superior NOMA/STAR-RIS architecture.

Chapter 3

System Model and Problem Formulation

This chapter presents the system model of the downlink STAR-IRS-assisted SISO-NOMA network considered in this thesis and formulates the corresponding optimization problem.

3.1 System Model Description

Let K denote the quantity of users within the system. Users are categorized into two distinct groups based on their spatial locations relative to the STAR-IRS. Anyone in the transmission zone gets the signal that was sent but then bent, while anyone in the reflection zone gets the signal that was mirrored. We denote the reflection-side user set by $\mathcal{K}_r$ and the transmission-side user set by $\mathcal{K}_t$, with cardinalities $|\mathcal{K}_r| = K_r$ and $|\mathcal{K}_t| = K_t$, respectively. These sets satisfy

$$\mathcal{K}_r \cap \mathcal{K}_t = \emptyset, \quad \mathcal{K}_r \cup \mathcal{K}_t = \{1, \ldots, K\}, \quad K = K_r + K_t.$$

User indices are arranged in ascending order corresponding to diminishing effective channel strength. User 1 has the best effective channel, whereas K has the weakest. Regardless of reflection or transmission zone, this ordering causes a set SIC decoding order for all users.

Each of the N passive components that make up the STAR-IRS controls its electromagnetic reaction to incoming signals on its own. Under low-resolution discrete phase-shift control, usually restricted to 2-bit quantization, each STAR-IRS element functions in accordance with hardware limitations and practical design concerns. This constraint significantly reduces implementation cost and energy consumption while maintaining sufficient beamforming flexibility for the considered SISO-NOMA setting.

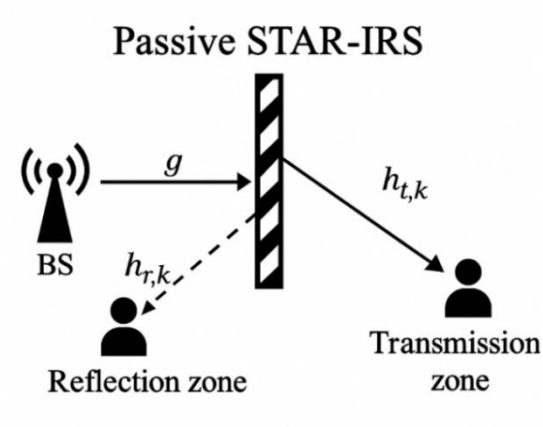

Figure 3.1: STAR-IRS assisted SISO-NOMA system model.

The overall STAR-IRS-assisted SISO-NOMA system, including the BS, the STAR-IRS and the two user groups on the reflection and transmission sides, is illustrated in Figure 3.1, which provides a visual aid for understanding the global topology and user distribution.

3.2 Channel and Link Modeling

In the STAR-IRS-assisted SISO-NOMA downlink communication system that is being looked at, each user gets messages from two different routes: one straight link from the BS and one secondary link through the STAR-IRS. For clarity, Figure 3.2 further highlights the link-level model for a generic user, including the BS–IRS channel g, the direct BS–user channel $h_{d,k}$, the STAR-IRS–user channel $h_{r,k}$, and the 2-bit quantized STAR-IRS elements. These figures jointly provide an intuitive picture of how the STAR-IRS cooperates with the BS to enhance coverage and signal quality.

We now characterize these links and construct the composite effective channels.

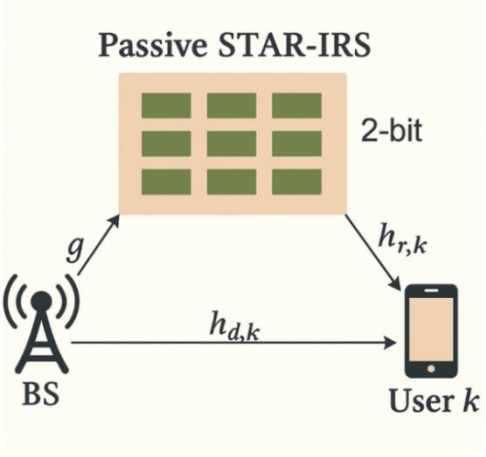

Figure 3.2: STAR-IRS-assisted SISO-NOMA communication system

3.2.1 Direct Link: Base Station to User Channel $h_{d,k}$

Let $h_{d,k} \in \mathbb{C}$ represent the complex scalar channel coefficient between user k and the BS. This direct connection is usually weaker than the STAR-IRS-assisted link because of the possibility of obstruction and significant route loss. However, this direct channel is kept in the overall received signal expression for modeling completeness and generality.

The large-scale path loss of the direct link is modeled using the standard log-distance model [46]

$$\mathrm{PL}(d) = \mathrm{PL}_0 - 10\alpha \log_{10}(d), \tag{3.1}$$

Here, PL_0 denotes the reference path loss at a distance of 1 meter, d represents the transmission distance between the base station and user k, and α signifies the path loss exponent. Small-scale fading is represented as a complex Gaussian random variable with a mean of zero and a variance of one, adjusted by the relevant route loss factor.

3.2.2 STAR-IRS Links: BS-IRS and IRS-User Channels

Let the STAR-IRS be composed of N passive elements. The channel from the BS to the IRS is represented by the vector

$$\boldsymbol{g} \in \mathbb{C}^{\mathrm{N}\times 1},$$

where the large-scale route loss and small-scale fading between the BS and the n-th STAR-IRS element are captured by the n-th element g_n. Every element g_n is represented as a complex Gaussian variable with Rayleigh distribution that is scaled by path loss dependent on distance.

Users are divided into two groups according on where they are in relation to the STAR-IRS [13]:

For a reflection-side user $k \in \mathcal{K}_r$, the STAR-IRS to user k is modeled by

$$\mathbf{h}_{r,k}^{(r)} \in \mathbb{C}^{N\times 1},$$

where the n-th element represents the link from the n-th STAR-IRS element to user k on the reflection side.

For a transmission-side user $k \in \mathcal{K}_t$, the STAR-IRS to user k is modeled by

$$\mathbf{h}_{r,k}^{(t)} \in \mathbb{C}^{N\times 1},$$

where the n-th element represents the link from the n-th STAR-IRS element to user k on the transmission side.

The elements of $\mathbf{h}_{r,k}^{(r)}$ and $\mathbf{h}_{r,k}^{(t)}$ are modeled as complex Gaussian variables with variances determined by the corresponding distances and propagation conditions.

3.2.3 STAR-IRS Phase Shift Matrices

The incident signal power may be divided between transmission and reflection by each STAR-IRS unit, and each component can receive a different phase shift. Two diagonal matrices are therefore used to represent the STAR-IRS configuration:

Reflection-phase matrix

$$\mathbf{\Theta}_r = \mathrm{diag}(\delta_1 e^{j\theta_1^r}, \delta_2 e^{j\theta_2^r}, \ldots, \delta_N e^{j\theta_N^r}),$$

Transmission-phase matrix

$$\mathbf{\Theta}_t = \mathrm{diag}((1-\delta_1) e^{j\theta_1^t}, (1-\delta_2) e^{j\theta_2^t}, \ldots, (1-\delta_N) e^{j\theta_N^t}),$$

where for the n-th STAR-IRS element:

$\delta_n \in [0,1]$ is the power-splitting factor between reflection and transmission,

θ_n^r and θ_n^t are the reflection and transmission phase shifts, respectively.

For practical low-complexity hardware, the phase shifts are constrained to a discrete 2-bit set [32, 33, 35, 36], i.e.,

$$\theta_n^r,\ \theta_n^t \in \left\{0, \frac{\pi}{2}, \pi, \frac{3\pi}{2}\right\}, \qquad \forall n = 1, \ldots, N\ .$$

3.2.4 Composite IRS-assisted Channels

Given the above definitions, the STAR-IRS-assisted channels for each user can be expressed as follows.

For a reflection-side user $k \in \mathcal{K}_r$, the cascaded channel is

$$h_k^{(r)} = \left(\mathbf{h}_{r,k}^{(r)}\right)^H \mathbf{\Theta}_r \mathbf{g}, \tag{3.2}$$

where $(\cdot)^H$ denotes the Hermitian transpose.

For a transmission-side user $k \in \mathcal{K}_t$, the cascaded channel is

$$h_k^{(t)} = \left(\mathbf{h}_{r,k}^{(t)}\right)^H \mathbf{\Theta}_t \mathbf{g}. \tag{3.3}$$

These cascaded channels show how the STAR-IRS phase configuration jointly shapes the reflection and transmission links by coherently combining contributions from all IRS elements.

3.2.5 Total Effective Channel

User k's effective channel comprises the direct BS–user connection and STAR-IRS-assisted link. We define

$$h_k^{\text{eff}} = \begin{cases} h_{d,k} + h_k^{(r)}, & k \in \mathcal{K}_r, \\ h_{d,k} + h_k^{(t)}, & k \in \mathcal{K}_t, \end{cases} \tag{3.4}$$

where $h_k^{(r)}$ and $h_k^{(t)}$ are given by (3.2) and (3.3), respectively.

Even though the direct link $h_{d,k}$ may be weak or partially blocked, it is retained in the model because, in certain geometries, it can still contribute non-negligibly to the received power and thus to the overall performance. This unified expression of h_k^{eff} also simplifies the subsequent derivation of SINR and rate expressions.

3.3 Joint Signal Modeling

The BS employs power-domain NOMA to simultaneously serve all K users using a single shared time-frequency resource block. Let $s_k \in \mathbb{C}$ denote the information-bearing symbol for user k , normalized such that

$$\mathbb{E}[|s_k|^2] = 1.$$

Let $p_k \geq 0$ be the power allocated to user k . The superposed transmit signal from the BS is

$$x = \sum_{k=1}^{K} \sqrt{p_k} s_k \,. \tag{3.5}$$

The total transmit power at the BS is therefore

$$P_{BS} = \sum_{k=1}^{K} p_k \,. \tag{3.6}$$

At user k , the received signal comprises the superposed NOMA signal propagated through the composite channel h_k^{eff} plus additive white Gaussian noise (AWGN). Denote the noise at user k by $n_k \sim \mathcal{CN}(0, \sigma^2)$. The received signal at user k can be expressed as

$$y_k = h_k^{\text{eff}} \sum_{j=1}^{K} \sqrt{p_j}\, s_j + n_k. \tag{3.7}$$

Expression (3.7) will be used to derive the SINR under the adopted SIC decoding strategy.

3.4 Detailed SINR Derivation

We adopt a fixed global SIC decoding order (Figure 3.4) based on the effective channel power gains of all users. Without loss of generality, we assume that users are indexed such that

$$\left|h_1^{\text{eff}}\right|^2 \geq \left|h_2^{\text{eff}}\right|^2 \geq \ldots \geq \left|h_K^{\text{eff}}\right|^2. \tag{3.8}$$

User K has the poorest effective channel, whereas user 1 has the greatest. In downlink NOMA, the smallest user (user K) decodes its own signal directly and sees all other users' signals as interference. Stronger users, on the other hand, decode and reject the signals of weaker users one by one before decoding their own signals.

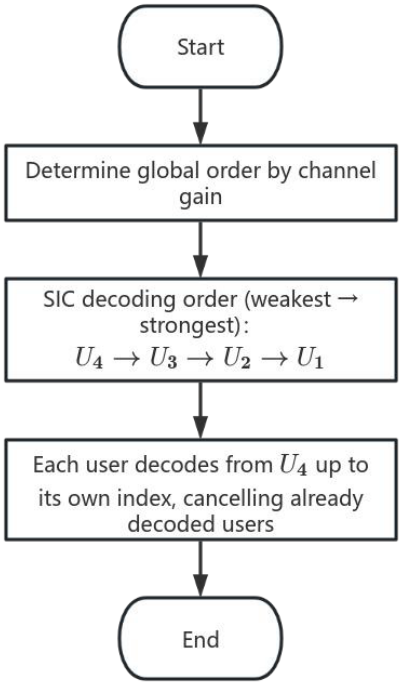

Figure 3.4: SIC decoding order example for NOMA.

3.4.1 SINR for Decoding a Weaker User's Signal

Consider a stronger user k attempting to decode the signal intended for a weaker user j, where $j>k$. At this stage of SIC, the signals of users with indices greater than j have already been decoded and subtracted, while the signals of users with indices $1,\ldots,j-1$ remain as interference. The SINR at user k when decoding user j's signal is given by

$$SINR_{k\rightarrow j} = \frac{p_j\left|h_k^{\text{eff}}\right|^2}{\sum_{\ell=1}^{j-1} p_\ell\left|h_k^{\text{eff}}\right|^2 + \sigma^2}, \qquad \forall\, 1 \leq k < j \leq K. \tag{3.9}$$

To ensure successful SIC decoding of user j's signal at user k, we require

$$SINR_{k\to j} \geq \gamma_j^{\min}, \qquad \forall\, 1 \leq k < j \leq K, \tag{3.10}$$

where $\gamma_j^{\min}$ is the minimum SINR (QoS) threshold associated with user j.

3.4.2 SINR for Decoding the Intended Signal

After user k has decoded and canceled all signals of weaker users $j > k$, it decodes its own signal while treating the signals of stronger users $\ell < k$ as residual interference. The SINR for decoding user k's own message is

$$SINR_k = \frac{p_k \left|h_k^{\text{eff}}\right|^2}{\sum_{\ell=1}^{k-1} p_\ell \left|h_k^{\text{eff}}\right|^2 + \sigma^2}, \qquad \forall k \in \{1, \ldots, K\}. \tag{3.11}$$

To guarantee the QoS requirement, this SINR must satisfy

$$SINR_k \geq \gamma_k^{\min}, \quad \forall k \in \{1, \ldots, K\}\,. \tag{3.12}$$

Equations (3.9)–(3.12) explicitly couple the power allocation variables $\{p_k\}$, the STAR-IRS configuration $(\boldsymbol{\Theta}_r, \boldsymbol{\Theta}_t)$, and the fixed SIC decoding order induced by $\left|h_k^{\text{eff}}\right|^2$.

3.5 Power Consumption Model

The total power consumption of the considered STAR-IRS-assisted SISO-NOMA system consists of two main components:

BS transmit power, required to superpose and broadcast all user signals;

STAR-IRS control power, consumed by the low-power circuits that realize discrete phase shifts at each element.

The BS transmit power is given by (3.6):

$$P_{BS} = \sum_{k=1}^{K} p_k. \tag{3.13}$$

Although the STAR-IRS is passive in the sense that it does not actively amplify RF signals, each of its N elements requires a small amount of power [8, 10-12, 49, 59, 60] to maintain its discrete phase state using low-power control circuits, such as PIN diodes or varactor-based tuning networks. Assuming that each element consumes a constant power P_{unit}, the total IRS control power is modeled as

$$P_{IRS} = N \cdot P_{unit}. \tag{3.14}$$

Therefore, the total system power consumption is

$$P_{total} = P_{BS} + P_{IRS} = \sum_{k=1}^{K} p_k + N \cdot P_{unit}. \tag{3.15}$$

This simple yet realistic model captures the trade-off between reducing BS transmit power and the fixed power overhead of controlling a STAR-IRS with many elements. It provides a suitable basis for the low-power optimization problem addressed below.

3.6 Optimization Constraints

To ensure reliable and energy-efficient operation, several practical constraints must be imposed on the system design. These constraints jointly capture power budget limits, user QoS requirement, SIC feasibility, and STAR-IRS hardware limitations.

(1) Total transmit power constraint

$$\sum_{k=1}^{K} p_k \le P_{\max}, \quad p_k \ge 0, \ \forall k. \tag{3.16}$$

(2) QoS SINR constraints

$$SINR_k \ge \gamma_k^{\min}, \quad \forall k, \tag{3.17}$$

with $SINR_k$ defined in (3.11).

(3) SIC feasibility constraints

$$SINR_{k\to j} \ge \gamma_k^{\min}, \quad \forall 1 \le k < j \le K, \tag{3.18}$$

with $SINR_{k\to j}$ defined in (3.9).

(4) Discrete phase-shift constraints

$$\theta_n^r, \theta_n^t \in \left\{0, \frac{\pi}{2}, \pi, \frac{3\pi}{2}\right\}, \quad \forall n = 1, \dots, N. \tag{3.19}$$

These constraints summarize the main physical and QoS requirement that any feasible configuration must satisfy.

3.7 Mathematical Problem Formulation

With the above definitions, the design variables of interest are

the power allocation vector $\mathbf{p} = [p_1, \dots, p_K]^T$;

the STAR-IRS reflection and transmission phase shifts $\{\theta_n^r, \theta_n^t\}_{n=1}^N$;

the power-splitting factors $\{\delta_n\}_{n=1}^N$.

The objective is to minimize the total system power consumption P_{total} in (3.15) while satisfying all QoS, SIC and hardware constraints. The resulting optimization problem can be written as

$$\min_{\{p_k\},\{\theta_n^r,\theta_n^t\},\{\delta_n\}} P_{total} = \sum_{k=1}^{K} p_k + N \cdot P_{unit}$$

$$\begin{aligned} \text{s.t.} \quad & SINR_k \geq \gamma_k^{\min}, \quad \forall k, \\ & SINR_{k\to j} \geq \gamma_k^{\min}, \quad \forall 1 \leq k < j \leq K, \\ & \textstyle\sum_{k=1}^{K} p_k \leq P_{\max}, \quad p_k \geq 0, \ \forall k, \\ & \theta_n^r, \theta_n^t \in \left\{0, \frac{\pi}{2}, \pi, \frac{3\pi}{2}\right\}, \quad \forall n \\ & 0 \leq \delta_n \leq 1, \quad \forall n. \end{aligned} \tag{3.20}$$

Due to the non-linear SINR expressions, the coupling between power allocation and STAR-IRS configuration, and the discrete phase-shift constraints, problem (3.20) is highly non-convex and difficult to solve optimally. In the next chapter, we develop an efficient alternating optimization framework, along with suitable relaxations and approximations, to obtain high-quality, low-complexity solutions suitable for practical STAR-IRS-assisted SISO-NOMA systems.

Chapter 4

Proposed Solution

4.1 Overview of the Optimization Framework

This chapter develops an optimization framework for minimizing the total power consumption of a STAR-IRS assisted SISO-NOMA downlink system. The overall power includes the BS transmit power as determined by NOMA power allocation under SINR constraints, as well as the static hardware power consumption of the STAR-IRS.

The joint optimization problem involves two tightly coupled components:

(1) power allocation at the BS, and

(2) STAR-IRS phase design on both reflection and transmission sides.

Because the SINR expressions depend nonlinearly on the STAR-IRS phase vectors, and the feasible set is non-convex under discrete phase constraints, the original problem is intractable. To address this, we decompose the formulation into two tractable subproblems and adopt an Alternating Optimization (AO) procedure that iteratively updates:

(1) BS power allocation with closed-form expressions, and

(2) STAR-IRS phase shifts using continuous refinement followed by quantization.

This AO scheme guarantees non-increasing objective values at each iteration and converges to a stationary point.

4.2 Power Allocation Subproblem

In this subsection we derive the optimal BS transmit powers for a fixed STAR-IRS configuration. For a given STAR-IRS phase profile, the effective channel of user k can be written as

$$h_k^{\text{eff}} = h_{d,k} + \mathbf{g}^H \mathbf{\Phi}_r \mathbf{h}_{r,k} + \mathbf{g}^H \mathbf{\Phi}_t \mathbf{h}_{t,k}, \tag{4.1}$$

where $h_{d,k}$ denotes the direct BS–user channel, $\mathbf{g}$ is the BS–IRS channel, $h_{r,k}$ and $h_{t,k}$ denote the IRS–user channels for the reflection and transmission regions, and $\mathbf{\Phi}_r$, $\mathbf{\Phi}_t$ are the corresponding diagonal phase-shift matrices.

For a fixed SIC decoding order from the weakest user K to the strongest user 1, the SINR requirement for user k to decode its own message is

$$SINR_k^{(k)} = \frac{\left|h_k^{\text{eff}}\right|^2 p_k}{\left|h_k^{\text{eff}}\right|^2 \sum_{j=1}^{k-1} p_j + \sigma^2} \geq \gamma_k^{\min}, \tag{4.2}$$

where p_k is the power allocated to user k, $\sigma^2$is the noise power, and $\gamma_k^{\min}$ is the QoS threshold.

In addition, user k must be able to decode the signal of every weaker user $i > k$ in the SIC chain. The corresponding SINR constraint is

$$SINR_k^{(i)} = \frac{\left|h_k^{\text{eff}}\right|^2 p_i}{\left|h_k^{\text{eff}}\right|^2 \sum_{j=1}^{i-1} p_j + \sigma^2} \geq \gamma_i^{\min}, \qquad 1 \leq k < i \leq K. \tag{4.3}$$

Because the effective channel magnitude $\left|h_k^{\text{eff}}\right|^2$ is fixed for a given STAR-IRS configuration, all constraints in (4.2)–(4.3) become linear constraints on the powers $\{p_k\}$. In a minimum-power design, every SINR constraint is active at the optimum; otherwise the corresponding power could be decreased without violating feasibility. Hence, the optimal powers satisfy equality conditions.

Starting from the weakest user K, which experiences only noise and no intra-cell interference, we obtain

$$p_K = \frac{\gamma_K^{\min} \sigma^2}{\left|h_K^{\text{eff}}\right|^2}. \tag{4.4}$$

For the next user $K - 1$, the interference comes from user K:

$$p_{K-1} = \frac{\gamma_{K-1}^{\min}}{\left|h_{K-1}^{\text{eff}}\right|^2} (\sigma^2 + \left|h_{K-1}^{\text{eff}}\right|^2 p_K). \tag{4.5}$$

More generally, for any user k, the optimal power can be expressed recursively as

$$p_k = \frac{\gamma_k^{\min}}{\left|h_k^{\text{eff}}\right|^2} (\sigma^2 + \left|h_k^{\text{eff}}\right|^2 \sum_{j=k+1}^{K} p_j), \qquad k = 1, \ldots, K. \tag{4.6}$$

By applying the recursion from $k = K$ up to $k = 1$, a closed-form power allocation for all users is obtained:

$$p_k^\star = f_k(\gamma_1^{\min}, \ldots, \gamma_K^{\min}, |h_1^{\text{eff}}|^2, \ldots, |h_K^{\text{eff}}|^2), \qquad k = 1, \ldots, K, \tag{4.7}$$

where $f_k(\cdot)$ denotes the explicit expression given by repeatedly applying (4.6). The exact representation is straightforward but omitted here for brevity.

For the considered STAR-IRS configuration, the resulting minimum transmit power at the BS is

$$P_{BS}(\phi) = \sum_{k=1}^{K} p_k^\star, \tag{4.8}$$

where ϕ collects all reflection and transmission phases. Including the static IRS control power defined in Chapter 3, the total system power becomes

$$P_{tot}(\phi) = P_{BS}(\phi) + NP_{IRS}, \tag{4.9}$$

which is now a scalar function of the STAR-IRS phase vector only and serves as the objective function for the phase-design subproblem [21-24].

4.3 STAR-IRS Phase Design Subproblem

With the closed-form power allocation derived above, the original joint optimization reduces to a phase-only problem. Substituting the optimal powers (4.7) into (4.8)–(4.9), the total power can be written as

$$\min_{\phi \in \mathcal{F}} P_{tot}(\phi), \tag{4.10}$$

where $\mathcal{F}$ denotes the discrete feasible set of STAR-IRS phase shifts containing both reflection and transmission phases for all N elements.

Problem (4.10) is highly non-convex because the phases affect the effective channels in (4.1), which then influence every term in the recursive expressions (4.4)–(4.7). Exhaustive search over all 4^{2N} combinations of 2-bit reflection and transmission phases is clearly infeasible for realistic values of N.

4.3.1 Continuous Relaxation and Quantization

In the first stage, each discrete phase variable is relaxed to a continuous variable on the unit circle, i.e.,

$$\phi_n \in [0, 2\pi], \quad n = 1, \ldots, 2N,$$

and the discrete constraint $\phi_n \in \mathcal{F}$ is temporarily ignored. Starting from an initial feasible phase vector $\boldsymbol{\phi}^{(0)}$, a local first-order descent update is computed as

$$\tilde{\boldsymbol{\phi}}^{(t+1)} = \boldsymbol{\phi}^{(t)} - \mu^{(t)} \nabla_{\boldsymbol{\phi}} P_{tot}(\boldsymbol{\phi}^{(t)}), \tag{4.11}$$

where $\mu^{(t)}$ is a step size obtained using a simple backtracking line search to ensure a sufficient decrease of the objective. In practice, the gradient can be approximated numerically by finite differences on each element.

Since the hardware only supports 2-bit phase resolution, each updated continuous phase must be projected back to the feasible set via nearest-neighbor quantization:

$$\phi_n^{(t+1)} = Q\left(\tilde{\phi}_n^{(t+1)}\right), \qquad \tilde{\phi}_n^{(t+1)} \in [0, 2\pi), \tag{4.12}$$

where $Q(\cdot)$ maps the angle to the closest value in $\left\{0, \frac{\pi}{2}, \pi, \frac{3\pi}{2}\right\}$.

To further improve performance under discrete constraints, a local refinement is applied to a small subset of "sensitive" elements whose phase perturbations lead to the largest changes in the objective. For each selected element, all alternative discrete values are tested and the best one (that yields the lowest P_{tot}) is kept. This step introduces negligible overhead but offers noticeable power savings.

4.3.2 Discrete Coordinate Descent

The second stage directly optimizes the discrete problem (4.10) without relaxation. At each iteration, one STAR-IRS element is selected and its discrete phase is optimized while keeping all other elements fixed. Denote by $\boldsymbol{\phi}_{-n}$ the phase vector excluding element n. For each candidate phase value $\phi_n \in \mathcal{F}$, the total power

$$P_{tot}(\phi_n, \boldsymbol{\phi}_{-n}) \tag{4.13}$$

is evaluated using the closed-form expressions in Section 4.2. The phase value that gives the smallest power is chosen and the algorithm proceeds to the next element.

After a complete sweep over all elements, the total power satisfies

$$P_{tot}(\boldsymbol{\phi}^{(t+1)}) \leq P_{tot}(\boldsymbol{\phi}^{(t)}), \tag{4.14}$$

which guarantees monotonic improvement. Although each sweep requires $\mathcal{O}(N|\mathcal{F}|)$ evaluations, the computational burden remains modest because each evaluation only requires scalar operations once the effective channels have been pre-computed.

The continuous-relaxation step provides a good starting point, while the discrete coordinate descent step refines the solution purely within the feasible set, yielding a high-quality phase configuration with low complexity [19, 22, 23, 29, 36].

4.4 Alternating Optimization Algorithm

Combining the closed-form power allocation and the hybrid phase optimization leads to the complete AO algorithm. A conceptual flowchart is shown in Figure 4.1, and the detailed pseudo-code is summarized below as Algorithm 1 [19-24, 26, 37, 38].

Algorithm 1 Alternating Optimization for STAR-IRS-Assisted NOMA

1: **Initialize:** Set iteration index $t = 0$, choose initial phase vector $\boldsymbol{\phi}^{(0)}$ (random or MRT-based), set convergence tolerance ε.

2: **Input:** STAR-IRS size N, user index set $\{1, \ldots, K\}$, QoS thresholds $\{\gamma_k^{\min}\}$, channel set $\{h_{d,k}, \mathbf{g}, \mathbf{h}_{r,k}, \mathbf{h}_{t,k}\}$.

3: **repeat**

4: For given $\boldsymbol{\phi}^{(t)}$, compute the effective channels h_k^{eff} for all users according to (4.1).

5: Using $\{h_k^{\text{eff}}\}$, compute the BS power allocation $\{p_k^{(t+1)}\}$ recursively from user K to user 1 according to (4.4)–(4.7), and obtain the corresponding total power $P_{tot}(\boldsymbol{\phi}^{(t)})$.

6: Using the updated powers $\{p_k^{(t+1)}\}$, perform the continuous phase update according to (4.11) to obtain the intermediate phase vector $\boldsymbol{\phi}^{cont}$.

7: Quantize and refine the phases by applying (4.12)–(4.14) over the STAR-IRS elements to obtain the updated discrete phase vector $\boldsymbol{\phi}^{(t+1)}$.

8: Set $t = t + 1$.

9: **until** Convergence criterion is met: $\left|P_{tot}(\boldsymbol{\phi}^{(t)}) - P_{tot}(\boldsymbol{\phi}^{(t-1)})\right| < \varepsilon$.

10: **Output:** Optimized phase vector $\boldsymbol{\phi}^{\star} = \boldsymbol{\phi}^{(t)}$ and BS power allocation $\{p_k^{\star}\} = \{p_k^{(t)}\}$.

4.5 Convergence and Complexity Analysis

The convergence of the proposed AO algorithm follows from two properties:

1. Optimal power update: For fixed STAR-IRS phases, the power allocation subproblem is solved optimally via the closed-form recursion (4.4)–(4.7). Therefore, step 2.1 of Algorithm 1 always yields the minimum feasible P_{BS} for the current $\boldsymbol{\phi}^{(t)}$.

2. Non-increasing phase update: The phase design step is constructed such that each update of ϕ does not increase the total power. Both the quantized gradient step and the coordinate descent refinement explicitly select phase values that reduce or keep unchanged P_{tot}.

Hence, if we denote the total power at iteration t by $P_{tot}^{(t)}$, the sequence satisfies

$$P_{tot}^{(0)} \geq P_{tot}^{(1)} \geq \ldots \geq P_{tot}^{(t)} \geq \ldots \geq 0. \tag{4.15}$$

Because the sequence is monotonically non-increasing and lower-bounded by zero, it converges to a finite limit. Due to non-convexity, the limit corresponds to a stationary (local optimum) solution, but the simulation results in Chapter 5 confirm that it already provides substantial performance gains over all benchmark schemes.

In terms of complexity, the power allocation step requires one sorting operation to determine the decoding order (once per channel realization) and then $\mathcal{O}(K)$ scalar operations to compute the recursion. The phase update step has complexity proportional to $\mathcal{O}(N)$ per gradient iteration and $\mathcal{O}(N|\mathcal{F}|)$ per coordinate-descent sweep. Overall, the total complexity scales approximately linearly with the number of users and STAR-IRS elements, making the proposed algorithm suitable for real-time or near real-time implementation.[22,23,26,38].

Chapter 5

Simulation and Results

5.1 Simulation Setup

This chapter evaluates the performance of the proposed STAR-IRS-assisted SISO-NOMA framework through numerical simulations. All channels follow the same Rician/Rayleigh propagation settings introduced earlier, and the BS, STAR-IRS, and user clusters are placed in a fixed geometry where reflection-side and transmission-side users occupy two semi-circular regions. One reference user is placed at the center of each region. The STAR-IRS employs 2-bit phase resolution for both reflection and transmission, and its hardware power consumption scales with the number of elements.

To compare the proposed method with practical and theoretical baselines, five schemes are evaluated:

No-IRS, Conventional IRS, Random STAR-IRS, Proposed Discrete STAR-IRS, and Continuous STAR-IRS (Upper Bound).

Each result is averaged over 200 independent channel realizations, with AO iteration limits following Chapter 4.

A complete list of simulation parameters is provided in Table 5.1 following similar settings as in [13, 17, 22, 25].

Item	**Value**
Carrier frequency/bandwidth	2.4 GHz/ 1MHz
Noise power	-104dBm
Path-loss exponents(α_{LOS},α_{NLOS})	(2.2,3.5)

Reference path loss PL_0	-30dB
Rician K-factor (BS-IRS, IRS-user)	8dB
BS-IRS default distance d_{BI}	25m
User cluster radius R	20m
Users per side (ref + random)	1+2
STAR-IRS phase resolution	2-bit$\{0,\pi/2,\pi,3\pi/2\}$
Per-element static power	2mW
Number of elements N (sweep)	{20,40,60,80,100}
QoS threshold γ (sweep)	{5,7,9,11,13}dB
Monte-Carlo (MC) realizations per point	200
AO iterations (discrete/continuous)	12/35
Convergence iterations shown	10

5.2 Simulation Results

This section gives numerical findings to illustrate the efficacy of the proposed STAR-IRS-assisted SISO-NOMA method. The performance is evaluated under the simulation settings described above and compared with the schemes defined in Section 5.1. The outcomes are averaged across 200 separate channel realizations, unless otherwise noted. The simulation results highlight the impact of STAR-IRS size, QoS requirement, IRS-user placement effect, asymmetry of user distribution, behavior of algorithm convergence and complexity of calculation.

A. Impact of STAR-IRS Size

Experiment 1 investigates the effect of the number of STAR-IRS elements on the sum power.

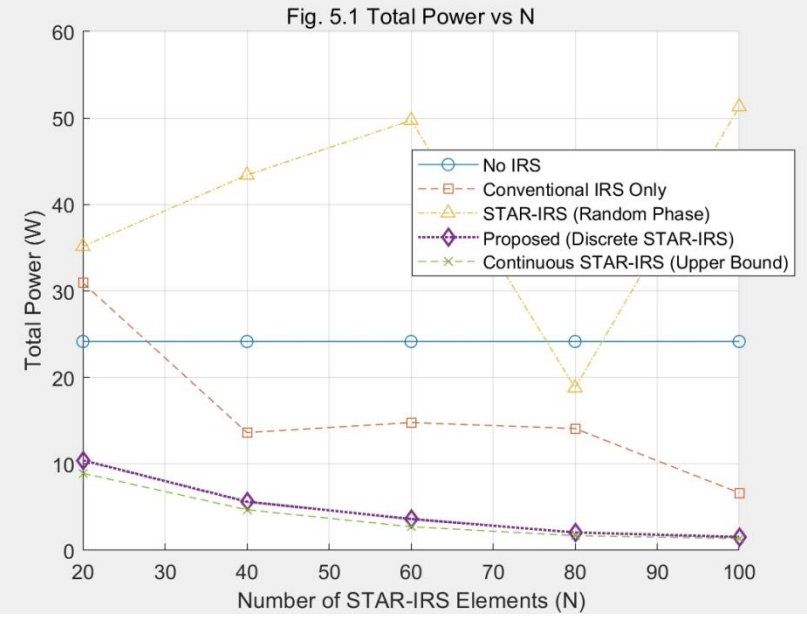

Figure 5.1: Total power consumption versus the number of STAR-IRS elements N for different schemes.

Figure 5.1 evaluates the impact of the number of STAR-IRS elements. At a representative configuration of $N = 60$, the proposed discrete STAR-IRS reduces the total transmit power by 84.97% and 75.44% compared with the No-IRS and conventional IRS-only baselines, respectively. It also outperforms the random-phase STAR-IRS by 92.70%, demonstrating the crucial role of optimized phase-shift design. Although a performance gap of 32.83% remains relative to the continuous-phase upper bound, this gap is acceptable given the significant reduction in hardware cost and computational complexity enabled by the 2-bit quantized STAR-IRS.

B. Impact of QoS Requirement

The second experiment evaluates how the system performance changes with different QoS thresholds γ.

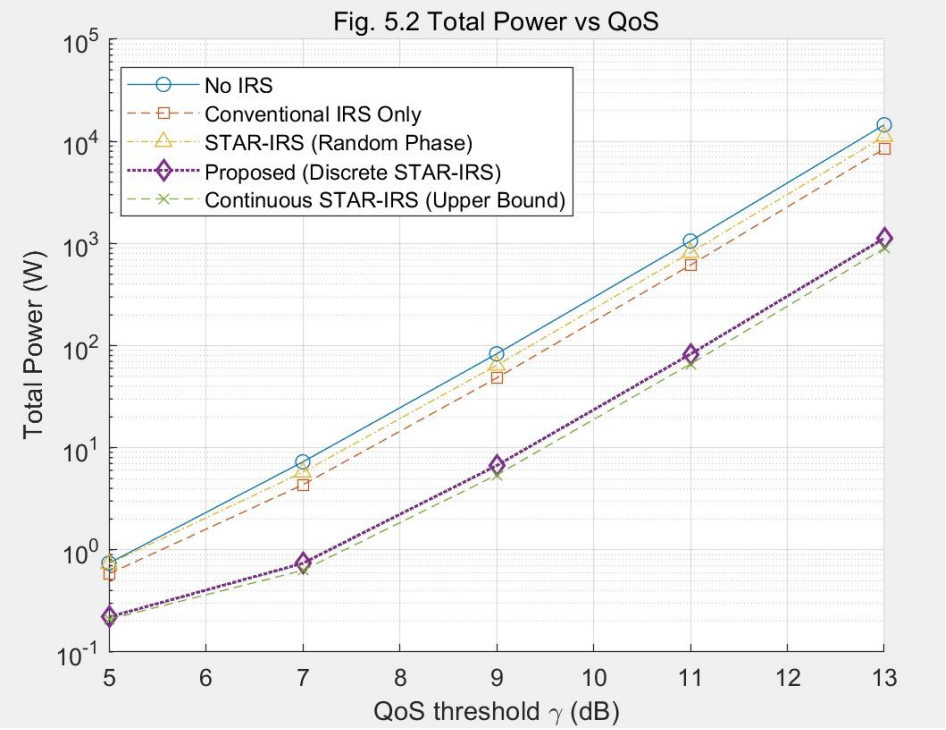

Figure 5.2: Total power consumption versus the QoS threshold γ for different schemes.

Figure 5.2 shows the variation of total power with respect to the QoS threshold. At a moderate QoS requirement of $\gamma = 9\text{dB}$, the proposed discrete design achieves 91.94% and 86.11% power savings over the No-IRS and conventional IRS-only schemes, respectively, while requiring only 23.71% more power than the continuous solution. These results confirm that the proposed discrete STAR-IRS enables energy-efficient QoS provisioning even under stringent SINR constraints.

C. Effect of STAR-IRS Placement Relative to Users

In the third set of results, the effect of moving the STAR-IRS farther away from the people on both sides of the surface is looked at.

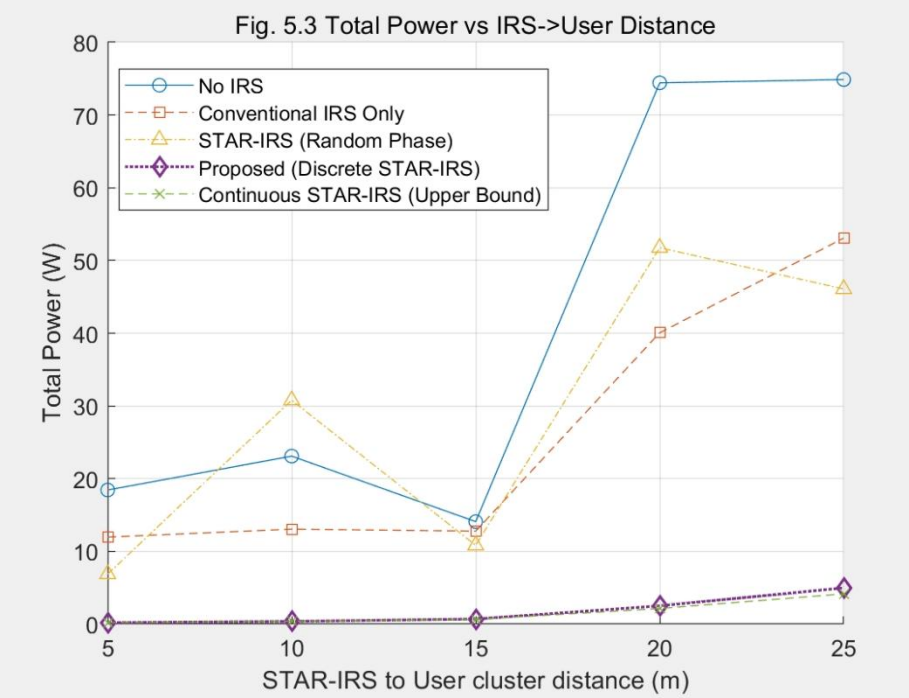

Figure 5.3: Total power consumption versus the STAR-IRS-to-user distance for different schemes.

Figure 5.3 investigates the IRS-to-user distance and highlights a key advantage of STAR-IRS. When the users are located at a moderate distance of $d_{IU} = 15\text{m}$, the proposed scheme offers extremely high power savings of 95.06% over No-IRS and 94.56% over conventional IRS-only. Moreover, the power gap to the continuous-phase benchmark is reduced to only 9.41%, showing that the refined discrete optimization achieves near-optimal performance under favorable deployment geometries [21-24].

D. Effect of STAR-IRS Placement Relative to the BS

The fourth experiment evaluates how the placement of the STAR-IRS relative to the BS influences the total power consumption.

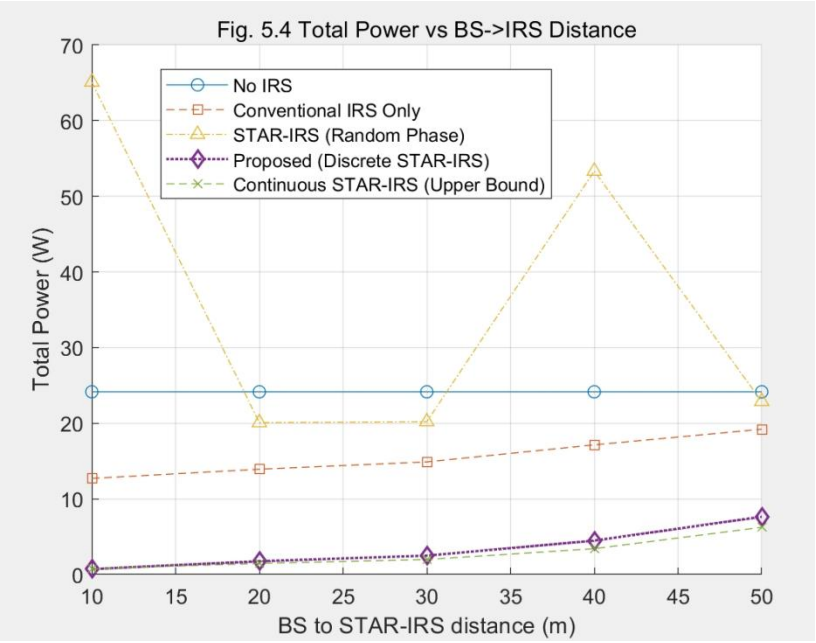

Figure 5.4: Total power consumption versus the BS-to-STAR-IRS distance for different schemes.

Figure 5.4 examines the STAR-IRS placement relative to the BS. At a balanced distance of $d_{BI} = 30\text{m}$, the proposed discrete STAR-IRS reduces power consumption by 89.67% and 83.24% compared with the No-IRS and conventional IRS-only baselines, respectively. The gap to the continuous-phase benchmark remains around 25.63%, consistent with observations in Fig. 5.1 and validating the robustness of the scheme with respect to placement variations.

E. Influence of Asymmetric User Distribution

The fifth experiment focuses on demonstrating the advantage of STAR-IRS over conventional reflecting-only IRS in two-sided user coverage scenarios.

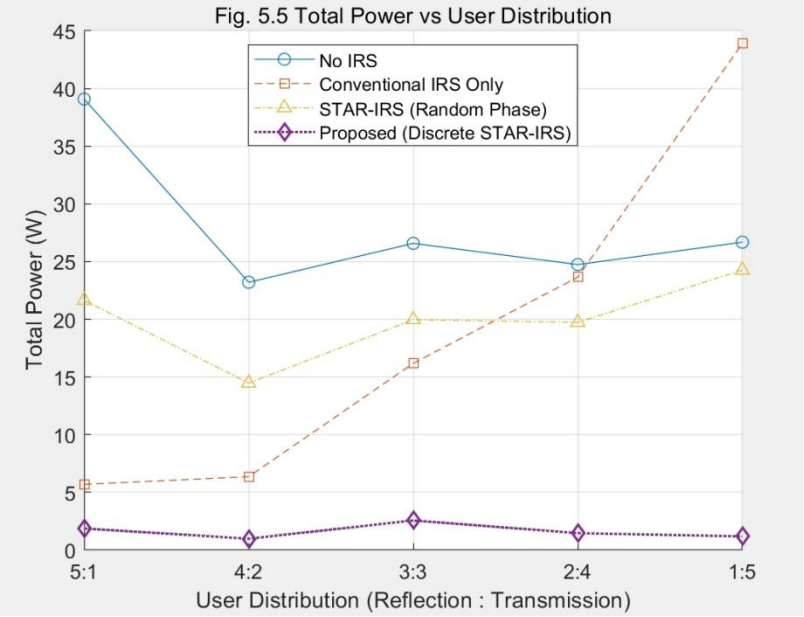

Figure 5.5: Total power consumption versus the user distribution across the reflection and transmission sides for different schemes

Figure 5.5 further verifies the dual-side transmission benefit under symmetric user distribution (3:3). The proposed design achieves 90.35% and 84.14% power savings relative to No-IRS and conventional IRS-only designs, respectively, while outperforming the random STAR-IRS by 87.15%. This confirms that STAR-IRS can achieve significant energy saving while simultaneously serving users on both sides of the surface without requiring additional active infrastructure.

F. Convergence Behavior of the Proposed Algorithm

We plot the variation of sum power about the change on the number of iterations of the alternating optimization algorithm to figure out how well the algorithm converges.

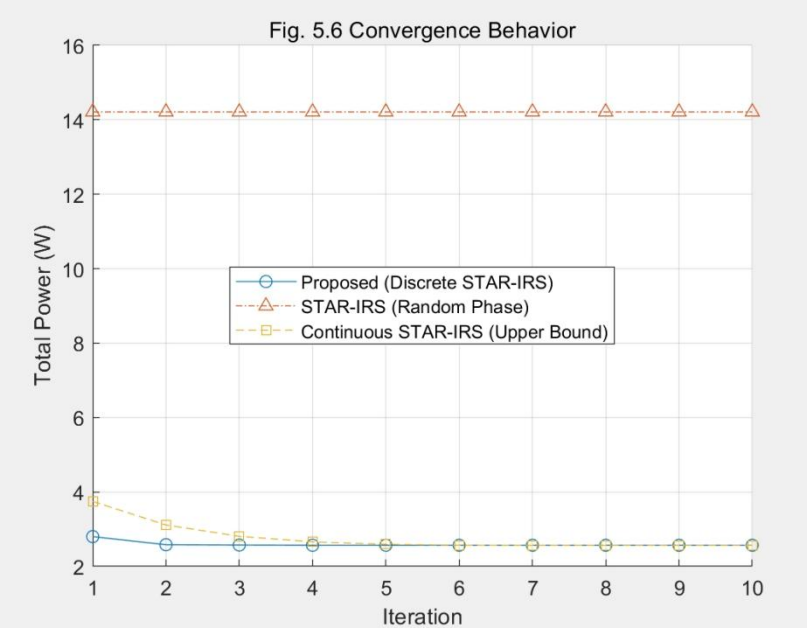

Figure 5.6: Convergence behavior of the proposed algorithm compared with benchmark schemes.

Figure 5.6 shows the convergence process of the proposed algorithm. The total transmit power is reduced from 2.8005W to 2.5671W, which is 8.33 percent in a few iterations. In short, it is only 0.11 percent more than the upper bound of the continuous phase [19, 22, 23], which means our proposed optimization can drive the discrete STAR-IRS to the near optimal operating point even with 2-bit quantization.

G. Computational Complexity Analysis

Finally, we use the average time per simulation at each IRS size to evaluate the computation efficiency of this method.

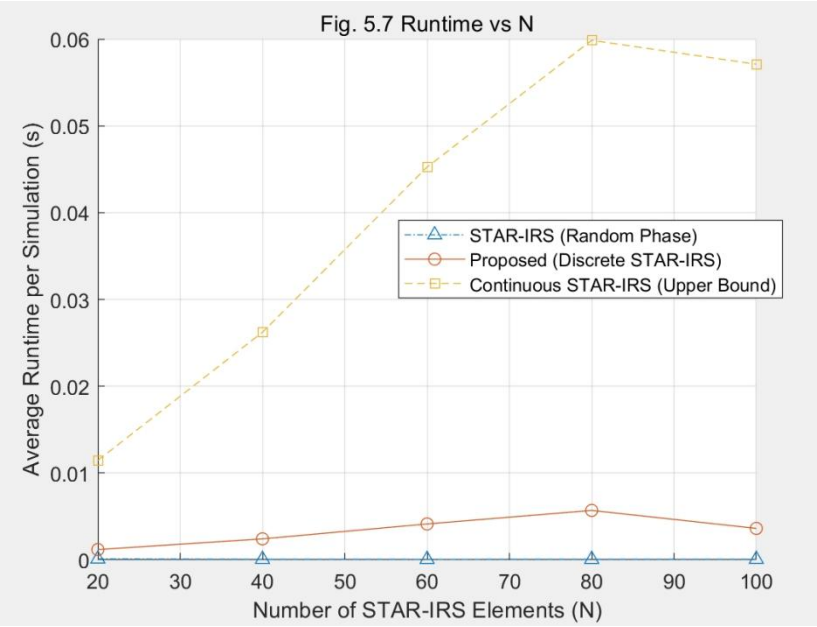

Figure 5.7: Average runtime per simulation versus the number of STAR-IRS elements N for different schemes.

Figure 5.7 compares the runtime scalability of different sizes of STAR-IRS. At the representative configuration of $N = 60$, the average continuous runtime of the proposed discrete STAR-IRS algorithm is 0.0042 seconds, which corresponds to a speed improvement of about 90.86% compared with the continuous-phase alternative (0.0457 seconds). At the same time, the introduced processing overhead of the proposed design is very slight compared to the single-trial random-phase baseline, and there is no optimization involved. These results indicate a good performance-complexity trade-off, so the algorithm can be applied in low-power 6G applications in practice.

5.3 Summary of Findings

This chapter studied the performance of the proposed power-efficient optimization framework of discrete STAR-IRS-assisted SISO-NOMA downlink transmission, which is applied to different representative deployment scenarios. The simulation results show that introducing the STAR-IRS can improve the channel quality of both the reflection user and the transmission user, and can achieve an aggressive power reduction that meets the users' QoS requirement. Compared with No-IRS, the proposed discrete STAR-IRS can reduce the total transmit power by 85-95 percent consistently under different STAR-IRS sizes, QoS requirement, geometric Settings and user spatial distributions. The performance improvement of the conventional reflective only IRS deployment is also significant. This results in 75-94%

less energy consumption than before, as the entire space will be covered on both sides. In addition, the performance gap of the proposed discrete optimization is still at the moderate level of 10% to 25% compared with the upper limit of the continuous-phase scheme, which is a reasonable trade-off in practical 2-bit hardware design.

In addition to energy efficiency, alternating optimization also performs well in terms of convergence and computing efficiency. The transmit power falls sharply after several iterations and the final power level is close to that of the continuous-phase reference, and the deviation is only 0.11% in typical channel conditions. The analysis of the runtime analysis results proves the practicability of the method, as can be seen from the results, with this proposed discrete STAR-IRS, we can achieve about one order of magnitude of acceleration in terms of the continuous phase optimization, while maintaining the advantages of the reconfigurable propagation.

In summary, the results confirm and demonstrate that the discrete STAR-IRS-assisted design is extremely good, simple but useful, and suitable for improving the power-efficient NOMA networks. These results demonstrate how to introduce discrete STAR-IRS into future 6G networks that prioritize sustainability and very large connectivity.

Chapter 6

Conclusion and Future Work

6.1 Conclusion

This thesis investigated the design of a power-efficient SISO-NOMA system assisted by a STAR-IRS capable of simultaneously serving users on both sides of the surface. A complete optimization framework was developed by combining closed-form NOMA power allocation with structured STAR-IRS phase design. The decomposition of the original coupled problem into a tractable alternating optimization form allowed efficient updates of transmit power and phase shifts, with convergence guaranteed by the monotonic improvement property established during the algorithm design.

Extensive simulations were conducted to verify the performance of the proposed method under various system conditions, including aperture size, QoS requirement, geometric configurations, and user distribution asymmetry. The results consistently demonstrated that the discrete STAR-IRS achieved substantial power savings compared with conventional IRS and random-phase STAR-IRS, while closely approaching the continuous-phase upper bound. The dual-sided STAR-IRS structure proved especially beneficial in asymmetric deployments where traditional single-sided IRS becomes inherently limited. Runtime measurements confirmed that the proposed discrete design remains practical even for moderately large surfaces.

Overall, the thesis provides both theoretical and numerical evidence that STAR-IRS, when combined with an efficient alternating optimization method, can significantly enhance the energy efficiency and flexibility of future downlink NOMA networks. The findings establish a viable and implementable path toward practical full-space intelligent surfaces for next-generation wireless systems [13, 21-26, 29-31].

6.2 Future Work

While the results in this thesis validate the potential of STAR-IRS for power-efficient NOMA transmission, several promising directions remain open for future exploration. One natural extension is to incorporate more refined hardware models [33-36, 40-45, 47-49, 61], such as amplitude–phase coupling, non-ideal energy leakage between reflection and transmission components, or element-group-based control architectures, which would bring the optimization framework closer to real hardware constraints. Extending the system to multi-antenna BSs or multi-cell cooperative scenarios [26, 37, 38, 51, 62, 63] would also enable spatial multiplexing and interference management capabilities beyond what a single-antenna baseline can offer.

Another promising direction is the integration of learning-based techniques [31, 37]. Since STAR-IRS channels may exhibit partial correlation or environmental regularity, data-driven or hybrid model-based learning strategies could reduce computation time or improve robustness under imperfect CSI. Finally, real-world deployment factors—such as user mobility, channel aging, sensing-assisted prediction, or joint communication–sensing operations—represent meaningful opportunities to adapt the algorithms developed here to dynamic and practical environments [40, 42, 46-49].

In summary, this work lays a rigorous foundation for STAR-IRS-assisted NOMA optimization and opens several avenues for further research to close the gap between theoretical performance and deployment-oriented designs.

Bibliography

[1] D. Sarkar, Yogita, S. S. Yadav, V. Pal, N. Kumar, and S. K. Patra, “A Comprehensive Survey on IRS-Assisted NOMA-Based 6G Wireless Network: Design Perspectives, Challenges and Future Directions,” IEEE Transactions on Network and Service Management, vol. 21, no. 2, pp. 2539–2562, Jan. 2024, doi: 10.1109/tnsm.2023.3348138.

[2] I. Budhiraja et al., “A Systematic Review on NOMA Variants for 5G and Beyond,” IEEE Access, vol. 9, pp. 85573–85644, 2021, doi: 10.1109/ACCESS.2021.3081601.

[3] M. Syed and Y. Li, “A Survey of NOMA: State of the Art, Key Techniques, Open Challenges, Security Issues and Future Trends,” arXiv.org, 2023. https://arxiv.org/abs/2306.06664.

[4] S. Sharma, K. Deka, and V. Bhatia, “Intelligent Reflecting Surface-Aided Downlink SCMA,” IEEE Systems Journal, vol. 17, no. 2, pp. 3204–3211, Jun. 2023, doi: 10.1109/jsyst.2022.3207998.

[5] M. Renzo et al., “Smart Radio Environments Empowered by Reconfigurable Intelligent Surfaces: How It Works, State of Research, and The Road Ahead,” IEEE Journal on Selected Areas in Communications, vol. 38, no. 11, 2020, doi: 10.1109/jsac.2020.3007211.

[6] X. Mu, J. Xu, Z. Wang, and Naofal Al-Dhahir, “Simultaneously Transmitting and Reflecting Surfaces for Ubiquitous Next Generation Multiple Access in 6G and Beyond,” Proceedings of the IEEE, vol. 112, no. 9, pp. 1–26, Jan. 2024, doi: 10.1109/jproc.2024.3405351.

[7] D. Renzo et al., “Smart Radio Environments Empowered by AI Reconfigurable Meta-Surfaces: An Idea Whose Time Has Come,” arXiv.org, 2019. https://arxiv.org/abs/1903.08925.

[8] C. Huang, A. Zappone, G. C. Alexandropoulos, M. Debbah, and C. Yuen, “Reconfigurable Intelligent Surfaces for Energy Efficiency in Wireless Communication | IEEE Journals & Magazine | IEEE Xplore,” ieeexplore.ieee.org, Jun. 19, 2019. https://ieeexplore.ieee.org/document/8741198.

[9] Q. Wu and R. Zhang, “Intelligent Reflecting Surface Enhanced Wireless Network via Joint Active and Passive Beamforming,” IEEE Transactions on Wireless Communications, vol. 18, no. 11, pp. 5394–5409, Nov. 2019, doi: 10.1109/twc.2019.2936025.

[10] K. Zhi, C. Pan, H. Ren, K. K. Chai, and M. Elkashlan, “Active RIS Versus Passive RIS: Which is Superior With the Same Power Budget?,” IEEE Communications Letters, vol. 26, no. 5, pp. 1150–1154, May 2022, doi: 10.1109/lcomm.2022.3159525.

[11] Z. Zhang et al., " Active RIS vs. Passive RIS: Which Will Prevail in 6G?," IEEE Transactions on Communications, vol. 71, no. 3, pp. 1707-1725, March 2023, doi: 10.1109/TCOMM.2022.3231893.

[12] R. Long, Y.-C. Liang, Y. Pei, and E. G. Larsson, “Active Reconfigurable Intelligent Surface-Aided Wireless Communications,” IEEE Transactions on Wireless Communications, vol. 20, no. 8, pp. 4962–4975, Aug. 2021, doi: 10.1109/twc.2021.3064024.

[13] X. Mu, Y. Liu, L. Guo, J. Lin, and R. Schober, “Simultaneously Transmitting and Reflecting (STAR) RIS Aided Wireless Communications,” IEEE Transactions on Wireless Communications, vol. 21, no. 5, pp. 3083–3098, May 2022, doi: 10.1109/twc.2021.3118225.

[14] Y. Liu et al., “STAR: Simultaneous Transmission and Reflection for 360° Coverage by Intelligent Surfaces,” IEEE Wireless Communications, vol. 28, no. 6, pp. 102–109, Dec. 2021, doi: 10.1109/mwc.001.2100191.

[15] M. Ahmed et al., “A Survey on STAR-RIS: Use Cases, Recent Advances, and Future Research Challenges,” IEEE Internet of Things Journal, vol. 10, no. 16, pp. 14689–14711, Aug. 2023, doi: 10.1109/jiot.2023.3279357.

[16] S. Zeng, H. Zhang, B. Di, Y. Liu, M. Di Renzo, Z. Han, H. V. Poor, and L. Song, “Intelligent omni-surfaces: Reflection-refraction circuit model, full-dimensional beamforming, and system implementation,” IEEE Transactions on Communications, vol. 70, no. 11, pp. 7711–7727, 2022.

[17] X. Yue and Y. Liu, “Performance Analysis of Intelligent Reflecting Surface Assisted NOMA Networks,” IEEE Transactions on Wireless Communications, vol. 21, no. 4, pp. 2623–2636, Apr. 2022, doi: 10.1109/twc.2021.3114221.

[18] Z. Ding and H. Vincent Poor, “A Simple Design of IRS-NOMA Transmission,” IEEE Communications Letters, vol. 24, no. 5, pp. 1119–1123, May 2020, doi: 10.1109/lcomm.2020.2974196.

[19] Z. Sun and Y. Jing, “On the Performance of Multi-Antenna IRS-Assisted NOMA Networks With Continuous and Discrete IRS Phase Shifting,” IEEE Transactions on wireless Communications, vol. 21, no. 5, pp. 3012–3023, Oct. 2021, doi: 10.1109/twc.2021.3117494.

[20] Z. Yang, P. Xu, G. Chen, Y. Wu, and Z. Ding, “Performance Analysis of IRS- Assisted NOMA Networks With Randomly Deployed Users,” IEEE Systems Journal, vol. 17, no. 2, pp. 1–12, 2022, doi: 10.1109/jsyst.2022.3195557.

[21] F. Fang, Y. Xu, Q.-V. Pham, and Z. Ding, “Energy-Efficient Design of IRS- NOMA Networks,” IEEE Transactions on Vehicular Technology, vol. 69, no. 11, pp. 14088–14092, Nov. 2020, doi: 10.1109/tvt.2020.3024005.

[22] J. Zhu, Y. Huang, J. Wang, K. Navaie, and Z. Ding, “Power Efficient IRS- Assisted NOMA,” IEEE Transactions on Communications, vol. 69, no. 2, pp. 900– 913, Feb. 2021, doi: 10.1109/TCOMM.2020.3029617.

[23] A. Ihsan, W. Chen, M. Asif, W. U. Khan, Q. Wu, and J. Li, “Energy-Efficient IRS-Aided NOMA Beamforming for 6G Wireless Communications,” IEEE Transactions on Green Communications and Networking, vol. 7, no. 1, pp. 1–1, 2022, doi: 10.1109/TGCN.2022.3209617.

[24] H. Wang, C. Liu, Z. Shi, Y. Fu, and R. Song, “On Power Minimization for IRS- Aided Downlink NOMA Systems,” IEEE Wireless Communications Letters, vol. 9, no. 11, pp. 1808–1811, Jun. 2020, doi: 10.1109/lwc.2020.2999097.

[25] X. Yue, J. Xie, Y. Liu, Z. Han, R. Liu, and Z. Ding, “Simultaneously Transmitting and Reflecting Reconfigurable Intelligent Surface Assisted NOMA Networks,” IEEE Transactions on Wireless Communications, vol. 22, no. 1, pp. 1– 1, 2022, doi: 10.1109/twc.2022.3192211.

[26] C. Wu, X. Mu, Y. Liu, X. Gu, and X. Wang, “Resource Allocation in STAR-RIS -Aided Networks: OMA and NOMA,” IEEE Transactions on Wireless Communications, vol. 21, no. 9, pp. 1–1, 2022, doi: 10.1109/twc.2022.3160151.

[27] X. Zhou, H. Wang, and J. Chen, “Joint Design of a Simultaneous Reflection and Transmission RIS in Mode-Switching Mode to Assist NOMA Systems,” Sensors, vol. 23, no. 12, pp. 5504–5504, Jun. 2023, doi: 10.3390/s23125504.

[28] X. Li, Y. Zheng, M. Zeng, Y. Liu, and O. A. Dobre, “Enhancing Secrecy Performance for STAR-RIS NOMA Networks,” IEEE Transactions on Vehicular Technology, vol. 72, no. 2, pp. 2684–2688, Feb. 2023, doi: 10.1109/tvt.2022.3213334.

[29] Y. Liu, Y. Wang, and W. Xu, “Beamforming Design for STAR-RIS-Assisted NOMA with Binary and Coupled Phase-Shifts,” Entropy, vol. 27, no. 2, p. 210, Feb. 2025, doi: 10.3390/e27020210.

[30] M. Asif, A. Ihsan, W. U. Khan, A. Ranjha, S. Zhang, and S. X. Wu, “Energy- Efficient Beamforming and Resource Optimization for AmBSC-Assisted Cooperative NOMA IoT Networks,” IEEE Internet of Things Journal, vol. 10, no. 14, pp. 12434–12448, Jul. 2023, doi: 10.1109/jiot.2023.3247021.

[31] A. Alqahtani, N. Taneja, A. Taneja, and N. Alqahtani, “Energy aware resource management in 6G IoT networks using STAR RIS,” Scientific Reports, vol. 15, no. 1, Jul. 2025, doi: 10.1038/s41598-025-05338-w.

[32] C. You, B. Zheng, and R. Zhang, “Intelligent Reflecting Surface with Discrete Phase Shifts: Channel Estimation and Passive Beamforming,” 2020 IEEE International Conference on Communications (ICC), Jun. 2020, doi: 10.1109/icc40277.2020.9149292.

[33] E. Wang et al., “A 1296-Cell Reconfigurable Reflect-Array Antenna With 2-bit Phase Resolution for Ka-Band Applications,” IEEE transactions on antennas and propagation, vol. 72, no. 4, pp. 3425–3437, Apr. 2024, doi: 10.1109/tap.2024.3368220.

[34] H. Yang et al., “A 1600-Element Dual-Frequency Electronically Reconfigurable Reflectarray at X/Ku-Band,” IEEE Transactions on Antennas and Propagation, vol. 65, no. 6, pp. 3024–3032, Apr. 2017, doi: 10.1109/tap.2017.2694703.

[35] H. Yang et al., “A Study of Phase Quantization Effects for Reconfigurable Reflectarray Antennas,” IEEE Antennas and Wireless Propagation Letters, vol. 16, pp. 302–305, Jan. 2017, doi: 10.1109/lawp.2016.2574118.

[36] L. Cao, H. Yin, L. Tan, and X. Pei, “RIS With Insufficient Phase Shifting Capability: Modeling, Beamforming, and Experimental Validations,” IEEE Transactions on Communications, vol. 72, no. 9, pp. 5911–5923, Sep. 2024, doi: 10.1109/tcomm.2024.3392784.

[37] R. Zhong, X. Mu, Y. Liu, Y. Chen, J. Zhang, and P. Zhang, “STAR-RISs Assisted NOMA Networks: A Distributed Learning Approach,” IEEE Journal of Selected Topics in Signal Processing, vol. 17, no. 1, pp. 264–278, Jan. 2023, doi: 10.1109/jstsp.2022.3229567.

[38] S. Syed, Wolfgang Utschick, and M. Joham, “Sum-Rate Optimisation of a Multi- User STAR-RIS-Aided System with Low Complexity,” 2025 IEEE 26th International Workshop on Signal Processing and Artificial Intelligence for Wireless Communications (SPAWC), pp. 1–5, Jul. 2025, doi: 10.1109/spawc66079.2025.11143284.

[39] Y. Feng, Q. Hu, K. Qu, W. Yang, Y. Zheng, and K. Chen, “Reconfigurable Intelligent Surfaces: Design, Implementation, and Practical Demonstration,” Electromagnetic Science, vol. 1, no. 2, pp. 1–21, Jun. 2023, doi: 10.23919/emsci.2022.0011.

[40] J. Tang, M. Cui, S. Xu, L. Dai, F. Yang, and M. Li, “Transmissive RIS for B5G Communications: Design, Prototyping, and Experimental Demonstrations,” IEEE Transactions on Communications, vol. 71, no. 11, pp. 6605–6615, Jul. 2023, doi: 10.1109/tcomm.2023.3292477.

[41] T. Huang, W. Fu, D. Lu, Y. Pan, M. Wang, and Y. Yan, “Wideband 1-bit reconfigurable transmission metasurface unit cell design in Ka-band with polarization hold and conversion,” Scientific Reports, vol. 13, no. 1, Nov. 2023, doi: 10.1038/s41598-023-47466-1.

[42] S. Gharbieh, J. Milbrandt, B. Reig, D. Mercier, M. Allain, and A. Clemente, “Design of a binary programmable transmitarray based on phase change material for beam steering applications in D-band,” Scientific Reports, vol. 14, no. 1, Feb. 2024, doi: 10.1038/s41598-024-53150-9.

[43] M. Xiang, Y. Xiao, J. Deng, S. Xu, and F. Yang, “Simultaneous Transmitting and Reflecting Reconfigurable Array (STAR-RA) With Independent Beams,” IEEE transactions on antennas and propagation, vol. 71, no. 10, pp. 8338–8343, Oct. 2023, doi: 10.1109/tap.2023.3291494.

[44] C. Zhang, Y. Luo, N. Yan, X. Guo, Y. Guo, and K. Ma, “A Reconfigurable Metasurface With Precise Phase Distribution for Both Transmission and Reflection Functions,” IEEE Transactions on Antennas and Propagation, vol. 72, no. 9, pp. 7154–7163, Sep. 2024, doi: 10.1109/tap.2024.3435525.

[45] J. L. Wu, Y. M. Pan, and S. Y. Zheng, “Design of Single-Layer Polarization- Dependent Transmissive and Reflective Focusing Metasurface,” IEEE Transactions on Antennas and Propagation, vol. 69, no. 11, pp. 7637–7646, Nov. 2021, doi: 10.1109/tap.2021.3076263.

[46] Z. Wang, L. Tan, H. Yin, K. Wang, X. Pei, and D. Gesbert, “A Received Power Model for Reconfigurable Intelligent Surface and Measurement-based Validations,” 2021 IEEE 22nd International Workshop on Signal Processing Advances in Wireless Communications (SPAWC), pp. 561–565, Sep. 2021, doi: 10.1109/spawc51858.2021.9593140.

[47] L. Dai et al., “Reconfigurable Intelligent Surface-Based Wireless Communications: Antenna Design, Prototyping, and Experimental Results,” IEEE Access, vol. 8, pp. 45913–45923, 2020, doi: 10.1109/ACCESS.2020.2977772.

[48] X. Pei et al., “RIS-Aided Wireless Communications: Prototyping, Adaptive Beamforming, and Indoor/Outdoor Field Trials,” IEEE Transactions on Communications, vol. 69, no. 12, pp. 8627–8640, Dec. 2021, doi: 10.1109/tcomm.2021.3116151.

[49] R. Song, H. Yin, Z. Wang, T. Yang, and X. Ren, “Modeling, Design, and Verification of an Active Transmissive RIS,” IEEE Transactions on Antennas and Propagation, vol. 72, no. 12, pp. 9239–9250, Oct. 2024, doi: 10.1109/tap.2024.3485183.

[50] S. Almaghthawi, E. Alsusa, and A. Al-Dweik, “On the Performance of IRS- Aided NOMA in Interference-Limited Networks,” IEEE Wireless Communications Letters, vol. 13, no. 2, pp. 560–564, Feb. 2024, doi: 10.1109/lwc.2023.3336800.

[51] Z. Li, W. Chen, Q. Wu, K. Wang, and J. Li, “Joint Beamforming Design and Power Splitting Optimization in IRS-Assisted SWIPT NOMA Networks,” IEEE Transactions on Wireless Communications, vol. 21, no. 3, pp. 2019–2033, Mar. 2022, doi: 10.1109/TWC.2021.3108901.

[52] X. Li, Z. Xie, Z. Chu, V. G. Menon, S. Mumtaz, and J. Zhang, “Exploiting Benefits of IRS in Wireless Powered NOMA Networks,” IEEE transactions on green communications and networking, vol. 6, no. 1, pp. 175–186, Mar. 2022, doi: 10.1109/tgcn.2022.3144744.

[53] M. Zeng, X. Li, G. Li, W. Hao, and O. A. Dobre, “Sum Rate Maximization for IRS-Assisted Uplink NOMA,” IEEE Communications Letters, vol. 25, no. 1, pp. 234–238, Jan. 2021, doi: 10.1109/lcomm.2020.3025978.

[54] Z. Ding, R. Schober, and H. V. Poor, “On the Impact of Phase Shifting Designs on IRS-NOMA,” IEEE Wireless Communications Letters, vol. 9, no. 10, pp. 1596– 1600, Oct. 2020, doi: 10.1109/lwc.2020.2991116.

[55] S. Xu, C. Liu, H. Wang, M. Qian, and J. Li, “STAR-RIS-assisted scheme for enhancing physical layer security in NOMA systems,” IET Communications, vol. 16, no. 19, Aug. 2022, doi: 10.1049/cmu2.12486.

[56] J. Xu, L. Yuan, N. Yang, N. Yang, and Y. Guo, “Performance Analysis of STAR -IRS Aided NOMA Short-Packet Communications With Statistical CSI,” IEEE transactions on vehicular technology, vol. 72, no. 9, pp. 12385–12390, Sep. 2023, doi: 10.1109/tvt.2023.3266830.

[57] Luxmi Kant Vishwakarma, R. Gour, S. Yadav, and A. Silva, “STAR-RIS-NOMA empowered vehicle-to-vehicle communications: Outage and ergodic capacity analysis,” Vehicular Communications, vol. 50, pp. 100852–100852, Oct. 2024, doi: 10.1016/j.vehcom.2024.100852.

[58] N. Khan and Y. H. Kim, “STAR-RIS Protocols for Throughput Maximization of Uplink NOMA,” 2024 15th International Conference on Information and Communication Technology Convergence (ICTC), pp. 915–916, Oct. 2024, doi: 10.1109/ictc62082.2024.10826882.

[59] M. Ahmed et al., “Active Reconfigurable Intelligent Surfaces: Expanding the Frontiers of Wireless Communication-A Survey,” IEEE Communications Surveys & Tutorials, vol. 27, no. 2, pp. 1–1, Jan. 2024, doi: 10.1109/comst.2024.3423460.

[60] L. Wu et al., “A Wideband Amplifying Reconfigurable Intelligent Surface,” IEEE Transactions on Antennas and Propagation, vol. 70, no. 11, pp. 10623– 10631, Nov. 2022, doi: 10.1109/TAP.2022.3187137.

[61] S. Y. Wang, Q. W. Zhang, X. H. Zhang, and Y. B. Li, “The Design of Wideband Nonreciprocal Transmission by Active Metasurface,” IEEE Antennas and Wireless Propagation Letters, vol. 22, no. 8, pp. 2012–2016, Aug. 2023, doi: 10.1109/lawp.2023.3271774.

[62] W. Ni, X. Liu, Y. Liu, H. Tian, and Y. Chen, “Resource Allocation for Multi- Cell IRS-Aided NOMA Networks,” IEEE Transactions on Wireless Communications, vol. 20, no. 7, pp. 4253–4268, Jul. 2021, doi: 10.1109/twc.2021.3057232.

[63] J. Wang, X. Tang, J. Liu, Z. Zhai, Q. Du, and N. Liu, “Multiple STAR-RISs- Empowered Multi-User Communications with Diversified QoS Provisioning,” IEEE Transactions on Vehicular Technology, pp. 1–6, 2025, doi: 10.1109/tvt.2025.3598381.

[64] A. Ahmed, X. Wang, A. Hawbani, W. Yuan, H. Tabassum, Y. Liu, M. U. F. Qaisar, Z. Ding, N. Al-Dhahir, A. Nallanathan, and D. W. K. Ng, " Unveiling the Potential of NOMA: A Journey to Next Generation Multiple Access," IEEE Commun. Surveys Tuts., vol. 27, pp. 3099-3164, 2025.

[65] Z. Wei, Y. Lei, D. W. K. Ng, J. Yuan, and L. Hanzo, " On the Performance Gain of NOMA over OMA in Uplink Communication Systems," IEEE Trans. Commun., vol. 68, no. 1, pp. 536-568, Jan. 2020.

[66] Z. Wei, D. W. K. Ng, J. Yuan, and H-M. Wang " Optimal Resource Allocation for Power-Efficient MC-NOMA with Imperfect Channel State Information," IEEE Trans. Commun., vol. 65, no. 9, pp. 3944-3961, Sep. 2017.

[67] X. Sun, N. Yang, S. Yan, Z. Ding, D. W. K. Ng, C. Shen, and Z. Zhong, " Joint Beamforming and Power Allocation in Downlink NOMA Multiuser MIMO Networks," IEEE Trans. Wireless Commun., vol. 17, no. 8, pp. 5367-5381, Aug. 2018.

[68] Y. Wang, J. Wang, D. W. K. Ng, R. Schober, and X. Gao, " A Minimum Error Probability NOMA Design," IEEE Trans. Wireless Commun., vol. 20, no. 7, pp. 4221-4237, Jul. 2021.

[69] Z. Wei, D. W. K. Ng, and J. Yuan, " Joint Pilot and Payload Power Control for Uplink MIMO-NOMA with MRC-SIC Receivers," IEEE Commun. Lett., vol. 22, no. 4, pp. 692-695, Apr. 2018.

[70] J. Zhang, J. Fan, J. Zhang, Q. Sun, D. W. K. Ng, and B. Ai, " Performance Analysis and Optimization of NOMA-Based Cell-Free Massive MIMO for IoT," IEEE Internet Things J., vol. 9, no. 12, pp. 9625-9639, 15 Jun., 2022.

[71] S. Li, Z. Wei, W. Yuan, J. Yuan, B. Bai, D. W. K. Ng, and L. Hanzo, " Faster-than-Nyquist Asynchronous NOMA Outperforms Synchronous NOMA," IEEE J. Sel. Areas Commun., vol. 40, no. 4, pp. 1128-1145, Apr. 2022.

[72] Z. Wei, D. W. K. Ng, and J. Yuan, " NOMA for Hybrid MmWave Communication Systems with Beamwidth Control," IEEE J. Sel. Topics Signal Process., vol. 13, no. 3, pp. 567-583, Jun. 2019.

[73] Z. Wei, L. Zhao, J. Guo, D. W. K. Ng, and J. Yuan, " Multi-Beam NOMA for Hybrid mmWave Systems," IEEE Trans. Commun., vol. 67, no. 2, pp. 1705-1719, Feb. 2019.

[74] Q. Wu, W. Chen, D. W. K. Ng, and R. Schober, " Spectral and Energy Efficient Wireless Powered IoT Networks: NOMA or TDMA?," IEEE Trans. Veh. Technol., vol. 67, no. 7, pp. 6663-6667, Jul. 2018.

[75] G. Chen, Q. Wu, W. Chen, D. W. K. Ng, and L. Hanzo, " IRS-aided Wireless Powered MEC Systems: TDMA or NOMA for Computation Offloading?," IEEE Trans. Wireless Commun., vol. 22, no. 2, pp. 1201-1218, Feb. 2023.

[76] Y. Cai, Z. Wei, S. Hu, C. Liu, D. W. K. Ng, and J. Yuan, " Resource Allocation and 3D Trajectory Design for Power-Efficient IRS-Assisted UAV-NOMA Communications," IEEE Trans. Commun., vol. 21, no. 12, pp. 10315-10334, Dec. 2022.

[77] Y. Feng, L. Xu, Q. Li, S. Yan, H. Wang, and D. W. K. Ng, " Transmit Rate Enhancement for STAR-RIS-Assisted Uplink NOMA," IEEE Trans. Veh. Technol., vol. 74, pp. 7651-7665, 2025.

[78] A. Singh, K. Singh, A. Kaushik, D. W. K. Ng, and S. Biswas, " Adaptive Neural Network Optimization for Fully Connected STAR-RIS-Aided NOMA Networks," IEEE ICC 2025 Workshop.

[79] R. Deshpande, M. Katwe, K. Singh, M.-L. Ku, and D. W. K. Ng, " Energy-Efficient STAR-RIS-aided MU-MIMO for Next-Generation URLLC Systems," IEEE Trans. Wireless Commun., vol. 23, no. 11, pp. 17807-17822, Nov. 2024.

[80] J. Zhang, S. Gong, W. Lu, C. Xing, N. Zhao, D. W. K. Ng, and D. Niyato, " Joint Design for STAR-RIS Aided ISAC: Decoupling or Learning," IEEE Trans. Wireless Commun., vol. 23, no. 10, pp. 14365-14379, Oct. 2024.

[81] C. Wang, C.-C. Wang, Z. Li, D. W. K. Ng, K.-K. Wong, N. Al-Dhahir, and D. Niyato, " STAR-RIS-Enabled Secure Dual-Functional Radar-Communications: Joint Waveform and Reflective Beamforming Optimization," IEEE Trans. Inf. Forensics Security, vol. 18, pp. 4577-4592, 2023.

[82] C. Liu, Y. Li, D. W. K. Ng, J. Yuan, and L. Dong, " Dual-Sided Active Intelligent Reflecting Surface-Enhanced Multi-Cell Communications," in Proc. of the IEEE International Conference on Communications (ICC), Jun. 2024, pp. 5527-5533.

[83] J. Wang, Y. Li, Y. Xia, X. Li, D. W. K. Ng, and O. A. Dobre, " Active STAR-RIS-Aided Wireless Powered Communication Networks," IEEE Trans. Wireless Commun., vol. 25, pp. 3406-3421, 2026.

[84] X. Zhou, F. Ke, C. Wu, X. Y. Zhang, and D. W. K. Ng, " Robust Beamforming for STAR-RIS aided Hybrid-Field ISAC Systems," IEEE Trans. Commun., vol. 74, pp. 5654-5669, 2026.

[85] R. Ranjan, M. V. Katwe, A. Bhattacharya, H. B. Mishra, K. Singh, and D. W. K. Ng, " A Robust STAR-RIS-assisted MU-MIMO System for Integrated Sensing and Communications," IEEE Trans. Cogn. Commun. Netw., vol. 12, pp. 2205-2220, 2026.

[86] X. Zhou, F. Ke, X. Y. Zhang, F. Gao, Y. Zhai, B. Tang, and D. W. K. Ng, " STAR-RIS-Aided Wideband Cell-Free ISAC: Joint Resource Allocation and Beamforming," IEEE Trans. Commun., doi: 10.1109/TCOMM.2026.3720330.

[87] E. Shi, Y. Zhu, J. Zhang, Z. Liu, C. Yuen, D. W. K. Ng, M. D. Renzo, and Bo Ai, " Joint Precoding and AP Selection for Energy-Efficient RIS-aided Cell-Free Massive MIMO with Multi-agent Reinforcement Learning," IEEE Trans. Wireless Commun., vol. 25, pp. 14719-14733, 2026.

[88] Y. Lu, J. Zhang, Y. Zhu, J. Zheng, D. Yang, D. W. K. Ng, and B. Ai, " Performance Optimization of RIS-Aided Cell-Free Massive MIMO Systems With DRL Approach," IEEE Trans. Wireless Commun., vol. 25, pp. 6711-6728, 2026.

[89] W. Wang, D. Qiao, L. Yang, Y. Zhan, and D. W. K. Ng, " Energy Efficiency Analysis of IRS-aided Wireless Communication Systems Under Statistical QoS Constraints: An Information-Theoretic Perspective," IEEE Trans. Wireless Commun., vol. 25, pp. 5077-5093, 2026.

[90] X. Zhang, D. Xu, J. Wang, S. Song, D. W. K. Ng, and M. Debbah, " Fluid Antenna Meets RIS: Random Matrix Analysis and Two-Timescale Design for Multi-User Communications," IEEE J. Sel. Areas Commun., vol. 44, pp. 1400-1416, 2026.

[91] B. Xu, J. Zhang, Z. Liu, Z. Wang, B. Ai, and D. W. K. Ng, " Asynchronous Distributed Beamforming for Beyond-Diagonal RIS-aided Movable Antenna Systems," IEEE Trans. Wireless Commun., vol. 25, pp. 4737-4751, 2026.

[92] L. Zhao, C. Sun, W. Ni, and D. W. K. Ng, " Reconfigurable Intelligent Surface-Aided Energy-Efficient Mobile Edge Computing in OFDM Systems," IEEE Commun. Lett., vol. 29, pp. 1446-1450, 2025.

[93] F. Xia, Z. Fei, J. Huang, X. Wang, R. Wang, W. Yuan, and D. W. K. Ng, " Sensing-enabled Predictive Beamforming Design for RIS-assisted V2I Systems: A Deep Learning Approach," IEEE Trans. Wireless Commun., vol. 23, no. 6, pp. 5571-5586, Jun. 2024.

[94] T.-X. Zheng, X. Chen, L. Lan, Y. Ju, X. Hu, R. Liu, D. W. K. Ng, and T. Cui, " Reconfigurable intelligent surface-aided secure integrated radar and communication systems," IEEE Trans. Wireless Commun., vol. 24, pp. 1934-1948, 2025.

[95] L. Yang, W. Zhang, P. S. Bithas, H. Liu, M. O. Hasna, T. A. Tsiftsis, and D. W. K. Ng, " Covert Transmission and Secrecy Analysis of RS-RIS-NOMA-Aided 6G Wireless Communication Systems," IEEE Trans. Veh. Technol., vol. 72, no. 8, pp. 10659-10670, Aug. 2023.

[96] S. Mondal, K. Singh, D. W. K. Ng, C.-P. Li, and Z. Ding, " Outage Performance of RIS-Aided NOMA ISAC Network for LEO Satellite System," IEEE ICC 2025 Workshop.

[97] L. Li, H. Li, Q. Li, S. Hao, X. Dai, and D. W. K. Ng, " Pattern-Domain NOMA-based Orthogonal Time Frequency Space Modulation," IEEE Trans. Veh. Technol., vol. 74, pp. 9370-9379, 2025.

[98] N. Li, P. Wu, L. Zhu, W. Mei, B. Ning, and D. W. K. Ng, " Sum-Rate Maximization for Movable-Antenna Array Enhanced Downlink NOMA Systems," accepted for publication, IEEE Trans. Wireless Commun., 2026.

[99] R. Zhang, K. Xiong, Y. Lu, D. W. K. Ng, P. Fan, and K. B. Letaief, " SWIPT-enabled Cell-Free Massive MIMO-NOMA Networks: A Machine Learning-based Approach," IEEE Trans. Wireless Commun., vol. 23, no. 7, pp. 6701-6718, Jul. 2024.

[100] Y. Wu, D. Xu, D. W. K. Ng, R. Schober, and W. Gerstacker, " Globally Optimal Resource Allocation Design for Discrete Phase Shift IRS-Assisted Multiuser Networks with Perfect and Imperfect CSI," IEEE Trans. Wireless Commun., vol. 24, pp. 1306-1324, 2025.

[101] J. An, C. Xu, Q. Wu, D. W. K. Ng, M. D. Renzo, C. Yuen, L. Hanzo, " Codebook-Based Solutions for Reconfigurable Intelligent Surfaces and Their Open Challenges," IEEE Wireless Commun., vol. 31, no. 2, pp. 134-141, Apr. 2024.

[102] Y. Chu, Z. Wei, Z. Yang, and D. W. K. Ng, " Channel Estimation for RIS-Aided MIMO Systems: A Partially Decoupled Atomic Norm Minimization Approach," IEEE Trans. Wireless Commun., vol. 23, no. 11, pp. 16048-16061, Nov. 2024.

[103] Y. Zhang, J. Zhang, H. Xiao, D. W. K. Ng, and B. Ai, " Channel Aging-Aware Precoding for RIS-Aided Wireless Communications," IEEE Trans. Veh. Technol., vol. 72, no. 2, pp. 1997-2008, Feb. 2023.

[104] J. Yao, J. Xu, W. Xu, D. W. K. Ng, C. Yuen, and X. You, " Robust Beamforming Design for RIS-aided Cell-free Systems with CSI Uncertainties and Capacity-limited Backhaul," IEEE Trans. Commun., vol. 71, no. 8, pp. 4636-4649, Aug. 2023.

[105] E. Shi, J. Zhang, J. Zheng, B. Ai, and D. W. K. Ng, " RIS-aided Cell-Free Massive MIMO Systems with Channel Aging," IEEE Trans. Veh. Technol., vol. 73, no. 8, pp. 11487-11502, Aug. 2024.

[106] Y. Sun, K. An, C. Li, Z. Lin, H. Niu, D. W. K. Ng, J. Wang, and N. Al-Dhahir, " Joint Transmissive and Reflective RIS-Aided Secure MIMO Systems Design under Spatially-Correlated Angular Uncertainty and Coupled PSEs," IEEE Trans. Inf. Forensics Security, vol. 18, pp. 3606-3621, 2023.

[107] W. Wang, L. Yang, Y. Zhan, D. Qiao, and D. W. K. Ng, " Robust Resource Allocation Design for Energy-efficient Active IRS-aided C-RSMA Systems," IEEE Trans. Commun., vol. 73, pp. 5168-5183, 2025.

[108] Y. Lu, J. Zhang, E. Shi, P. Zhang, D. W. K. Ng, D. Niyato, and B. Ai, " Energy-Efficient RIS-Aided Cell-Free Massive MIMO Systems: Application, Opportunities, and Challenges," IEEE Wireless Commun., vol. 32, pp. 148-155, 2025.

[109] P. Zhang, J. Zhang, H. Xiao, X. Zhang, D. W. K. Ng, and B. Ai, " Joint Distributed Precoding and Beamforming for RIS-Aided Cell-Free Massive MIMO Systems," IEEE Trans. Veh. Technol., vol. 73, no. 4, pp. 5994-5999, Apr. 2024.

[110] R. Zhang, K. Xiong, Y. Lu, P. Fan, D. W. K. Ng, and K. B. Letaief, " Energy Efficiency Maximization in RIS-assisted SWIPT Networks with RSMA: A PPO-based Approach," IEEE J. Sel. Areas Commun., vol. 41, no. 5, pp. 1413-1430, May 2023.

[111] Y. Cao, C. Xing, Y. Wu, J. An, D. W. K. Ng, and X.-G. Xia, " RIS-Assisted Massive Access with Semi-Passive Elements," IEEE Trans. Wireless Commun., vol. 23, pp. 10546-10561, 2024.

[112] S. Lin, Y. Zou, and D. W. K. Ng, " Ergodic Throughput Maximization for RIS-Equipped-UAV-Enabled Wireless Powered Communications With Outdated CSI," IEEE Trans. Commun., vol. 72, no. 6, pp. 3634-3650, Jun. 2024.